Investigation into the extrudability of a new Mg-Al-Zn-RE alloy with large amounts of alloying elements

Bai, Sheng Wen; Fang, Gang; Zhou, Jie

DOI
10.1007/s11661-019-05242-9

Publication date
2019

Document Version
Accepted author manuscript

Published in
Metallurgical and Materials Transactions A: Physical Metallurgy and Materials Science

Citation (APA)
Bai, S. W., Fang, G., & Zhou, J. (2019). Investigation into the extrudability of a new Mg-Al-Zn-RE alloy with large amounts of alloying elements. *Metallurgical and Materials Transactions A: Physical Metallurgy and Materials Science*, *50*(7), 3246-3264. https://doi.org/10.1007/s11661-019-05242-9

Investigation into the extrudability of a new Mg-Al-Zn-RE alloy with large amounts of alloying elements

Sheng-Wen Bai[1], Gang Fang[1,*], Jie Zhou[2]

[1] State Key Laboratory of Tribology, Department of Mechanical Engineering, Tsinghua University, Beijing 100084, China

[2] Department of Biomechanical Engineering, Delft University of Technology, Mekelweg 2, 2628 CD Delft, The Netherlands

*Corresponding author, Gang Fang: Tel: +86-10-6278 2694, E-mail: fangg@tsinghua.edu.cn

Abstract

The present study was aimed to determine the extrudability of a newly developed Mg-Al-Zn-RE magnesium alloy with large amounts of alloying elements. The experimental and numerical investigation clearly showed that the extrudate temperature was a crucial factor deciding if a critical temperature between 754 K and 768 K (481 °C and 495 °C) was reached during extrusion, above which hot shortness occurred. Under the extrusion conditions applied, dynamic recrystallization (DRX) occurred, leading to grain refinement from a mean grain size of 165 μm in the as-solid-solution-treated billet to 8.0-10.9 μm in the extruded rods. Second-phase particles, such as $Mg_{17}Al_{12}$ and $Al_{11}La_3$, were found to distribute on grain boundaries and aid in grain refinement. The mechanical properties of the extrudate were greatly influenced by the as-extruded microstructure and extrusion condition. As the initial billet temperature decreased, the ultimate tensile strength (UTS) and elongation of the alloy increased, while yield strength (YS) remained almost unchanged. At an initial billet temperature of 523 K (250 °C), a stem speed of 3.93 mm/s and a reduction ratio of 29.8, the extruded magnesium alloy had a mean grain size of 8.0 μm. Its YS, UTS and elongation reached 217±3 MPa, 397±7 MPa and 20±1.3%, respectively.

Keywords: magnesium; extrusion; microstructure; mechanical property; hot shortness

1. Introduction

Since the beginning of this century, magnesium alloys, the lightest structural metallic materials, have attracted great attention for applications in 3-C (computers, communications and consumer electronics) products, automobiles and aerospace in order to realize weight reduction [1-6]. Cast magnesium alloy parts made by using a variety of casting techniques have been widely accepted for these applications [7]. However, the applications of wrought magnesium alloys have been rather limited, although in general wrought magnesium alloys possess better mechanical properties than the cast counterpart and are thus more suitable for structural applications [8-9]. Extruded magnesium alloy products, for example, accounted for less than 3% of the annual output of magnesium production in 2013 [10]. The limited applications of extruded products are mainly due to the low extrudability of magnesium alloys, compared to aluminum alloys, leading to low productivity and low cost-effectiveness.

The limited use of extruded magnesium alloy products is also due to the achievable mechanical properties that are not substantially better than those of the cast counterpart. In recent years, a lot of research efforts have been made to improve the mechanical properties and extrudability of magnesium alloys.

Basically, there are two ways to improve the mechanical properties of extruded magnesium alloys. Alloying is effective in enhancing the mechanical properties of magnesium, but at the same time imposes limitations to applicable extrusion speed, as a result of raised resistance to hot deformation, increased temperature rise during the process and lowered incipient melting point. Microstructure control throughout materials processing from casting to extrusion is also effective, especially the control of grain structure within an applicable extrusion process window by applying an optimum combination of extrusion process parameters. Obviously, it is the best if alloying and microstructure control are combined to achieve optimum mechanical properties from a refined grain structure and from the distribution of fine precipitates at a minimum loss in extrusion speed.

The effect of alloying on the microstructure, extrudability and mechanical properties of extruded magnesium alloy products depends on the amount of a chosen element and its solubility in the magnesium matrix. When its content is low, it stays dissolved in the magnesium matrix even at room temperature, creating a solid solution strengthening effect. However, when the content exceeds its solubility in the magnesium matrix, second-phase particles precipitate as temperature decreases, creating a precipitation strengthening effect and possibly contributing to a refined grain structure as well by pinning grain boundaries, which in turn strengthens the alloy further. These strengthening mechanisms may operate individually or in combination. The mechanical properties of extruded magnesium were, for example, shown to be improved through the addition of Al and Zn by a combination of strengthening mechanisms, depending on the contents of these elements [11]. Yin et al. [12] found that the addition of Zn refined the grain structure of an extruded Mg-Zn-Mn alloy and led to an improved yield strength. In Mg-5Sn-xZn alloys (x=1, 2, 4), the amounts of Mg_2Sn and MgZn particles increased with increasing Zn content, which contributed to the mechanical properties of the extruded magnesium alloys through precipitation strengthening [13]. Small amounts of Ca were found to be able to refine the grain structure and improve both the tensile strength and elongation of Mg-Al-Zn and Mg-Zn alloys [14, 15]. Rare earth (RE) elements, such as Gd, Y and Ce, were added to different extruded magnesium alloys to enhance their mechanical properties [16-21]. For example, Y improved the mechanical properties of Mg-Zn-Zr alloys through grain refinement and the formation of the I-phase (Mg_3Zn_6Y). However, an excessive addition of Y to the alloys led to the formation of the W-phase ($Mg_3Zn_3Y_2$), which decreased the strengths. Actually, it is the ratio of Y to Zn (wt. %) that determines the volume fraction of the I-phase and its strengthening effect [18].

Zeng et al. [22] also demonstrated that the polygon-shaped Mg_3Zn_6Y phase played an important role in strengthening the extruded magnesium alloy Mg-6Zn-1.5Y-0.5Zr. Stanford et al. [23] found that the strength of magnesium was greatly improved by adding 0.22-4.65% Gd, owing to the mechanisms of recrystallized grain refinement and solution strengthening. Zhang et al. [24] revealed that the synthetic additions of Ca, Ce and La to the Mg-6.0Zn alloy resulted in the refinement of secondary phases and precipitates, promoting the pining effect to restrict grain growth and the dispersion strengthening effect. Homma et al. [25] developed a high-strength magnesium alloy Mg-1.8Gd-1.8Y-0.7Zn-0.2Zr with an ultimate tensile strength (UTS) of 542 MPa and a 0.2% proof stress of 473 MPa. The high strengths were achieved thanks to fine precipitates formed during aging subsequent to hot extrusion. Yamasaki et al. [26] found that the yield strength of the warm-extruded magnesium alloy Mg-Zn-2.5Gd reached a high level of 345 MPa, because of the refinement of grains and the dispersion of a precipitate with a long period ordered (LPO) structure. Chen et al. [27] investigated the effect of Nd addition on the microstructures and mechanical properties of the Mg-6Al-2Ca-*x*Nd (x=0, 1, 2, 3, 4 and 5 wt.%) alloys. With increasing content of Nd, the amounts of Al_2Nd and Al_3Nd phases increased, while the amount of $Mg_{17}Al_{12}$ decreased. The presence of the Al-Nd compounds contributed to the refinement of the recrystallized grain structure formed during hot extrusion, leading to an enhanced yield strength. Therefore, it is critically important to understand the strengthening phase formed in RE-containing magnesium alloys and its sizes, volume fraction and distribution.

On the other hand, as mentioned earlier, with the addition of alloying elements to magnesium, the extrudability usually decreases [11]. Luo et al. [28], for example, found that the incipient melting point of the magnesium alloy AZ31 was 371 K (98 °C) lower than that of AM30 due to the presence of Zn in the former. It means that AZ31 is more susceptible to hot shortness. To prevent hot shortness from occurring, a lower initial billet temperature must be considered, if extrusion speed and reduction ratio are desired to be fixed. As a result, the extrusion pressure required for the process will be higher. If the force capacity of the available extrusion press is not enough, extrusion speed or reduction ratio must be reduced in order to lower the pressure requirement, leading to sacrifice in extrusion productivity. In the case of high-strength magnesium alloys with large amounts of alloying elements, more severe limitations are imposed on the applicable extrusion conditions. For each alloy, its extrusion window must be specifically defined in order to avoid hot shortness and achieve the highest possible extrusion productivity in combination with the consideration on the microstructure and mechanical properties desired to achieve.

During hot extrusion, the main process parameters, i.e., initial billet temperature, extrusion speed and reduction ratio, may all influence the microstructure of an extruded magnesium alloy. The mechanical properties of the alloy depend on its microstructural characteristics, such as grain size, the intensity of texture and the distribution of second-phase particles [29-33]. Murai et al. [29] found that fine grains in the extruded magnesium alloy AZ31 were obtained at a low initial billet temperature and a low extrusion speed, resulting in high mechanical properties of the extrudate. Ishihara et al. [30] reported that at a given initial billet temperature of 693 K (420 °C) and extrusion speed of 5 m/min, the mean grain size of the extruded magnesium alloy AZ31 increased from 30 to 170 μm, when reduction ratio was increased from 10 to 100. Zhang et al. [31] investigated the effect of the initial billet temperature on the microstructure and mechanical properties of the extruded Mg-1.0Zn-0.5Ca alloy. They found that with decreasing initial billet temperature from 673 K to 603 K (400 °C to 330 °C), the mean grain size decreased from 25 to 2.5 μm and the ultimate tensile strength (UTS) increased from 201 to 300 MPa. Tong et al. [32] found that the basal texture of the Mg-5.3Zn-0.6Ca alloy was weakened at a higher extrusion speed, which resulted in a lower tensile yield strength. Park et al. [33] demonstrated that the temperature rise occurring during extrusion increased the solubility of Sn in the magnesium matrix and thereby reduced the volume fraction of Mg_2Sn precipitates in the Mg-Sn-Al-Zn extrudate, resulting in a low strength. Therefore, the choice of extrusion parameters is of critical importance for the achievable mechanical properties of an extruded magnesium alloy.

Indeed, many of recent research efforts have aimed at achieving the highest possible strength through optimizing extrusion condition, often in combination with modification of alloy composition. By performing extrusion at an extrusion ratio of 44, a ram speed of 60 mm/min and billet temperature of 623 K (350 °C), for example, Shahzad et al. [34] obtained the ultimate tensile strength (UTS) of 328 MPa for the magnesium alloy AZ80. Chen et al. [35] found that the UTS of the extruded magnesium alloy Mg-5.3Zn-1.13Nd-0.51La-0.28Pr-0.79Zr could reach 325-350 MPa, when the billet temperature applied was 523 K (250 °C). Singh et al. [36] developed the extruded magnesium alloys Mg-6*x*Zn-*x*Y (*x*=0.2, 0.35 and 0.5 at. %) with UTS varying from 397.8 to 418.6 MPa and elongation values over 12%. Park et al. [37] reported that the UTS of the Mg-9Al-0.6Zn alloy reached 375 MPa after extrusion at a billet temperature of 523 K (250 °C), extrusion speed of 1 mm/s and a reduction ratio of 7.35. Bu et al. [38] developed a new magnesium alloy containing large amounts of alloying elements, including La and Gd (Mg-Al-Zn-RE). The effects of La and Gd on the microstructure and mechanical properties of the extruded alloy were extensively investigated. The results showed that, as a result of La and Gd additions, the $Al_{11}La_3$, Al_8Mn_4Gd and Al_3Gd phases were present in the extruded alloy in addition to the $Mg_{17}Al_{12}$ phase. During extrusion, particle stimulated nucleation (PSN) occurred due to the presence of abundant second-phase particles, leading to the formation of fine, recrystallized grains. The alloy had a UTS of 397 MPa, being higher than that of the traditional magnesium alloy AZ80, owing to a combination of grain refinement strengthening, precipitation strengthening, solid-solution strengthening, dislocation strengthening and subgrain strengthening. Therefore, the alloy was considered to be highly promising for aircraft applications. However, the effects of extrusion process parameters on the microstructure and mechanical properties of the alloy were not investigated. As microstructural changes, such as dynamic recrystallization and precipitation, are largely governed by the local thermomechanical conditions during hot extrusion, it was hypothesized that the as-extruded microstructure and resultant mechanical properties, especially elongation (10%) [38], would be optimized through optimizing the extrusion condition.

The present work concerned a case study on the extrudability, microstructure evolution during extrusion and the resulting mechanical properties of the newly developed magnesium alloy Mg-Al-Zn-RE. It was intended to serve as an example to show how to determine the extrudability of a new magnesium alloy and understand the effect of extrusion condition on its microstructure and mechanical properties through a combination of experimental research and numerical simulation using the finite element (FE) method. The extrusion experiments were performed by using a tailor-designed die setup. Different combinations of extrusion parameters, namely initial billet temperature, extrusion speed and reduction ratio, were employed. FE simulations of hot extrusion were carried out to predict the extrudate temperature that was hard to measure accurately in real extrusion operation. In addition, the effects of extrusion parameters on the microstructure evolution and mechanical properties of the alloy were investigated through microstructure observation and tensile tests of the extrudate.

2. Material, extrusion experiments and numerical simulations

2.1 Material

The nominal chemical composition of the newly developed Mg-Al-Zn-RE alloy is given in Table 1. The alloy was designed on the basis of AZ81 [38], which is known for having a very narrow range of applicable deformation conditions [39]. The addition of the rare earth elements (i.e., La and Gd) tended to lower its workability further. Hot compression tests indeed showed that this alloy was extraordinarily prone to hot shortness; hot cracking occurred at temperatures higher than 693 K (420 °C). To push the temperature limit upwards, the as-cast alloy was solid-solution-treated at 693 K (420 °C) for 24 h, following by water quenching, in order to dissolve second-phase particles, such as $Mg_{17}Al_{12}$ that has an incipient melting point of 710 K (437 °C) [40]. The solution treatment was also intended to homogenize the as-cast microstructure and improve its extrudability. Cylindrical billets with a diameter of 29 mm and lengths of 23 and 15 mm were prepared for extrusion experiments.

Table 1. Chemical composition (wt. %) of the Mg-Al-Zn-RE alloy.

Element	Al	Zn	Mn	La	Gd	Mg

Chemical composition (wt. %)	8.0~8.8	0.3~0.8	0.15~0.3	0.7~1.3	0.3~0.7	Bal.

2.2 Hot compression tests

A constitutive model of the magnesium alloy is needed for the FE simulations of extrusion. To determine the constitutive constants, uniaxial compression tests of cylindrical specimens with sizes of $\phi 8 \times 12$ mm were performed by using a Gleeble 1500 thermomechanical simulator. Test temperatures from 573 K to 693 K (300 °C to 420 °C) and with an interval of 30 K (30 °C) were chosen. Strain rates selected were 0.001, 0.01, 0.1, 1 and 10 s^{-1}. The flow stress-strain curves obtained at different temperatures and strain rates are shown in Fig. 1. The hyperbolic sine-type equation (Eq. 1), proposed by Sellars and McTegart [41], was adopted to describe the deformation behavior of the material.

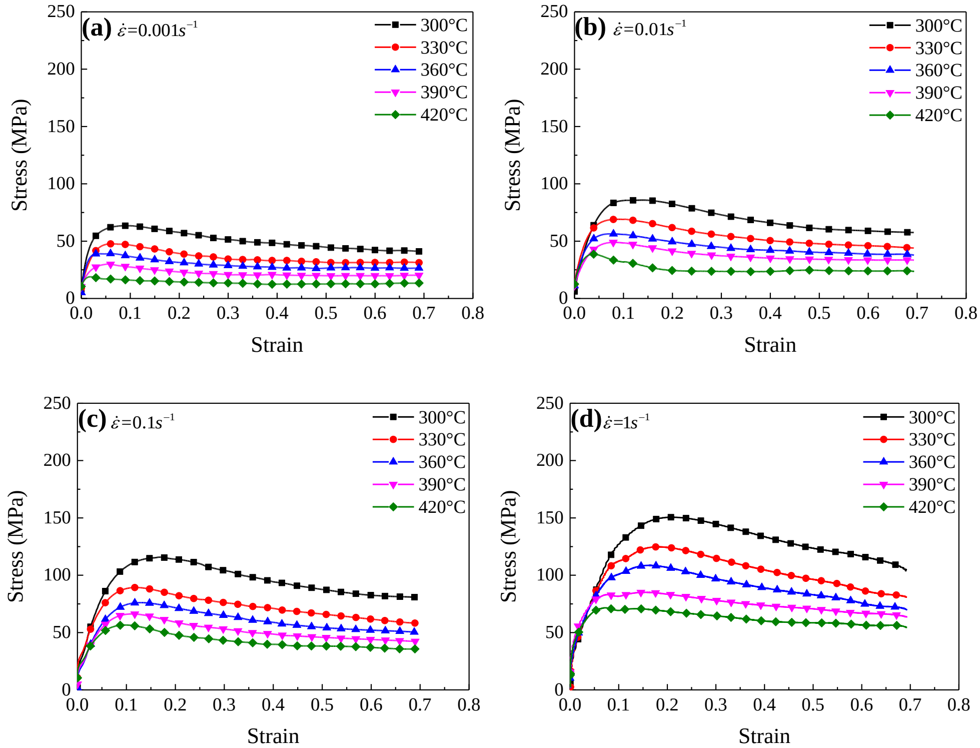

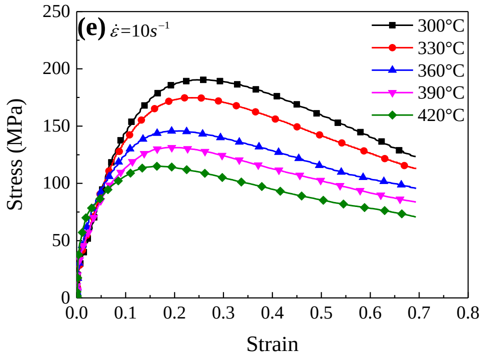

Fig. 1. Flow stress-strain curves of the magnesium alloy at temperatures from 573 K to 693 K (300 °C to 420 °C) and strain rates (a) 0.001 s^{-1}, (b) 0.01 s^{-1}, (c) 0.1 s^{-1}, (d) 1 s^{-1} and (e) 10 s^{-1}.

$$\dot{\varepsilon}=A[\sinh(\alpha\sigma)]^{n}\exp\left(\frac{-Q}{RT}\right) \tag{1}$$

where, A, α and n are material constants, Q is the activation energy for hot deformation, and R is the gas constant. The constitutive constants obtained were used as material constants in the model for the FE simulations of extrusion (Table 2).

Table 2. Constitutive constants of the magnesium alloy (Mg-Al-Zn-RE).

Constitutive constant	A	α	n	Q (kJ/mol)
Value	2.3188e+10	1.721e-2	4.5164	141.329

2.3 Extrusion tooling setup

The tooling setup, specially designed for this research, consisted of a structural supporting framework, a heating system, a die with a round opening, a container, a stem and a stem holder (Fig. 2). The supporting framework included a fastening plate, supporting rods and a supporting plate, which were used to fix the die setup on the platform of a press driven by a hydraulic system. The stem holder was connected to the crosshead of the hydraulic press. Four resistance-heating elements with a total power of 2000 W were employed to heat the container, extrusion die and billet. Heating was controlled by a PID (Proportion Integration Differentiation) controller based on the feedback temperature measured by Thermocouple 1. Thermocouple 2 was inserted into the die to measure the temperature near the die orifice during extrusion. The measuring point was 2 mm away from the die bearing (Fig. 2b).

Two extrusion dies with orifice diameters of 5.5 and 4.2 mm were employed for extrusion at reduction ratios of 29.8 and 51.0, respectively, while the diameter of the container liner stayed unchanged (30 mm). For each die, the inlet angle was 60° and the length of straight die bearing was 1 mm.

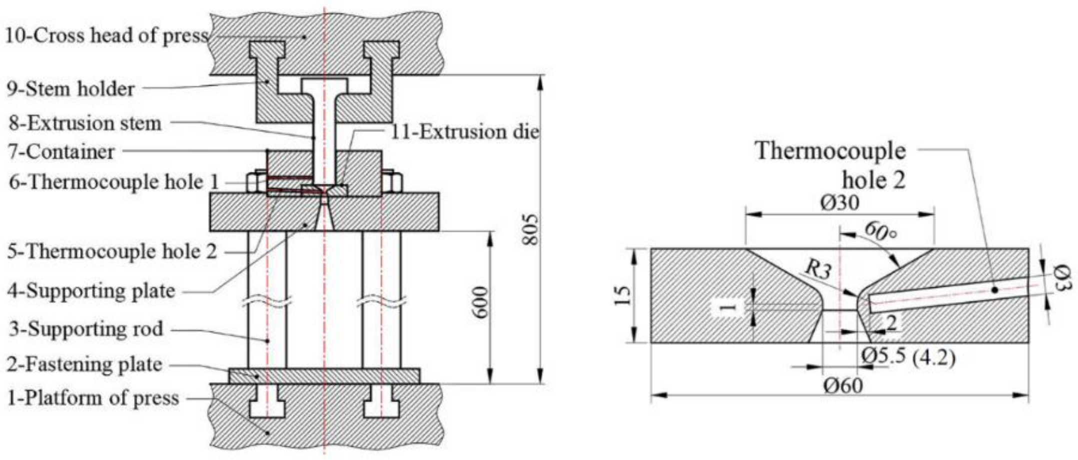

(a) (b)

Fig. 2. Tooling set-up to extrude rods: (a) schematic and (b) dimensions of one of the extrusion dies.

2.4 Extrusion experiments

Extrusion experiments were performed by using the tooling setup mounted on a hydraulic press with a force capacity of 2 MN. Before extrusion, the billet was heated to a preset temperature at a rate of 8 K/min (8 °C/min) and socked for 15 min. The container and die were heated to the same temperature as the billet. During extrusion, the temperature near the die orifice was measured by Thermocouple 2. After extrusion, the extruded rod was cut off from the discard and air-cooled. Initial billet temperature, extrusion speed and reduction ratio were taken as the main process variables. Initial billet temperature was set at 523, 573, 623, 673 and 713 K (250, 300, 350, 400 and 440 °C). Stem speed increased from 0.48 mm/s to 8.24 mm/s. Reduction ratios were 29.8 and 51.0, as mentioned in Subsection 2.3.

2.5 Microstructure observation

Samples were cut from the extruded rods along the longitudinal extrusion direction (Fig. 3). The exposed surfaces were ground and mechanically polished. An etchant composed of 5 g picric acid, 10 ml acetic acid, 10 ml deionized water and 100 ml absolute ethyl alcohol was used to etch the samples. The microstructures of the samples were observed using an optical microscope (Zeiss Axio Scope.A1) and a scanning electron microscope (SEM, FEI Quanta 200 FEG) equipped with an energy dispersive x-ray spectroscope (EDS). The grain sizes of the extrudate were determined by using the linear intercept method. The sizes and volume fractions of second-phase particles were measured by using the commercial software Image-Pro Plus on the basis of SEM micrographs.

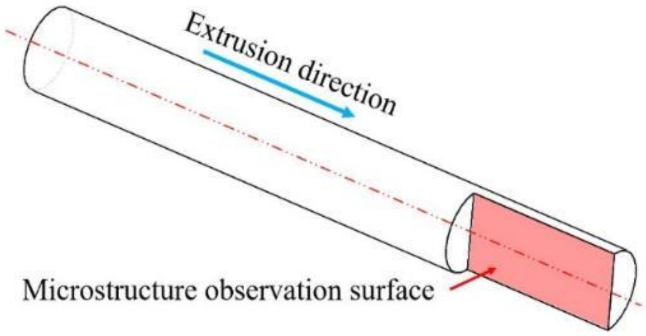

Fig. 3. Schematic of the longitudinal section of an extruded rod for microstructure observation.

2.6 Tensile tests

Tensile specimens were prepared by machining from the extruded rods. They had a total length of 90 mm, a gauge length of 25 mm and a gauge diameter of 4 mm, conforming to the standard GB/T 228.1-2010. Tensile tests were conducted using a universal material testing machine (AG-X, Shimadzu) at a crosshead speed of 1 mm/min. Tensile force was applied in the direction being the same as the extrusion direction. The test of the specimen processed under each condition was repeated at least twice to ensure the reproducibility of the data.

2.7 Finite element simulations

FE simulations were performed to predict the temperature of the extrudate at the die orifice, as affected by the extrusion variables. An axisymmetric FE model (Fig. 4) was built by using the commercial software package DEFORM. The billet, extrusion die, stem and container were all meshed to be composed of quadrilateral elements. The billet was defined as a thermo-rigid-plastic material, and the thermomechanical effect occurring during extrusion was taken into account. The extrusion tools were considered to be rigid objects and heat transfer was allowed. The constitutive equation (Eq. 1) was applied in the FE simulations. The initial temperatures of the container and die were set to be the same as those used in the extrusion experiments, while the stem was set at an initial temperature of 293 K (20 °C). Heat exchanges between the billet, extrusion tooling and surrounding environment were taken into consideration. A shear friction model was adopted at the interfaces between the billet and extrusion tooling and the friction coefficient was set at 1.0 [42]. The physical properties of the magnesium alloy and tooling material (H13 tool steel) are listed in Table 3 [43].

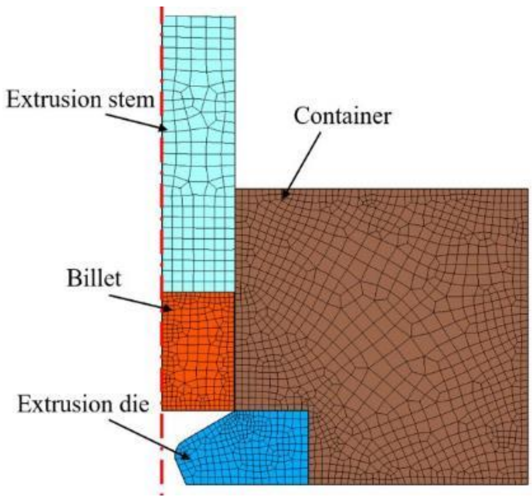

Fig. 4. Axisymmetric FE model to simulate the extrusion process to produce rods.

Table 3. Physical properties of the billet and extrusion tooling.

Physical property	Magnesium alloy	H13 tool steel

Thermal conductivity (W/(m °C))	96	28.4
Heat capacity (N/(mm^2 °C))	2.097at 600 K (327°C) 2.275 at 800 K (527°C)	5.6
Heat transfer coefficient between tooling and workpiece (N/(°C s mm^2))	11	11
Heat transfer coefficient between tooling/workpiece and air (N/(°C s mm^2))	0.02	0.02
Emissivity	0.7	0.7

3. Results and discussion

3.1 Extrudate temperature

The extrudate temperature at the die exit, the most important process parameter that strongly influences the surface quality and microstructure of the extrudate, depends on the initial billet temperature, extrusion speed and reduction ratio. It is however difficult to measure directly and accurately. To verify the extrudate temperature predicted from FE simulations, comparisons with the temperatures near the die bearing, measured by inserted Thermocouple 2, were made. Fig. 5a shows an example of the predicted temperature distribution inside the extruded billet, rod, and extrusion tooling, when the initial billet temperature was 573 K (300 °C), reduction ratio 51.0 and stem speed 1.92 mm/s. The temperature predicted at point P1 inside the die reached a peak value of 600 K (327 °C) at a stem displacement of 15 mm. It was very close to the value of 598 K (325 °C) measured by Thermocouple 2. In addition, the calculated and measured temperature evolutions at point P1 during extrusion were compared. The results (Fig. 5b) showed that the simulated temperatures were in agreement with the experimentally measured values. The differences between simulated and measured temperatures were negligible. It indicated that the present FE model of extrusion was reliable in temperature calculation. Based on this fact, we considered the calculated temperature at point P2 to be the exact temperature of the extrudate surface. In addition, a large difference in temperature between the extrudate surface (678 K, i.e., 405 °C at point P2) and measuring point (600 K, i.e., 327 °C at point P1) was found, even though there was a distance of only 2 mm between these two points. It confirmed that the measured die temperature could not be used as the temperature of the extrudate directly.

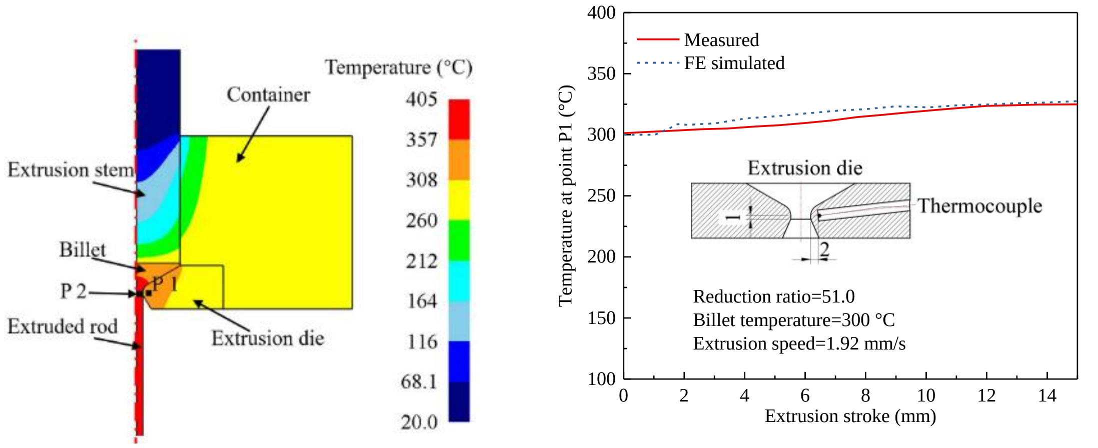

(a) (b)

Fig. 5. Predicted temperature distribution inside the billet, extrudate and extrusion tooling (a) and comparison between the measured and predicted temperatures at P1 along with stem displacement (b).

Fig. 6 shows the FE simulated temperature evolutions at point P2 under different extrusion conditions. At the initial stage of extrusion, the temperature at point P2 rose significantly, which was attributed to heat generation from both plastic deformation and severe friction between the billet and tooling. The temperature rise due to deformation heating can be described by using Eq. 2, where η is the adiabatic factor with a value between 0.9 and 0.95, and ρ is the specific density and C_{p} is the specific heat [44].

$$\Delta T = \frac{\eta \int \sigma \mathrm{d}\varepsilon}{\rho C_{\mathrm{P}}} \tag{2}$$

Eq. 3 gives the shear-type friction model employed during the simulations, where τ is the shear stress, and m is the friction factor [45]. The friction factor was set to be 1, considering the severe friction between the tooling and billet [42]. The frictional heating contributed to temperature rise during the extrusion process. In the meantime, heat was transferred between the billet and tooling and dissipated into the atmosphere. With rising extrudate temperature, more heat was transferred from the extrudate to the tooling. Heat generation and dissipation to the die competed with each other, and then the extrudate temperature reached a steady state.

$$\tau = \frac{m\sigma}{\sqrt{3}} \tag{3}$$

Fig. 7 shows the simulated temperatures at point P2, when two different friction factor values of 0 and 1 were applied. The same reduction ratio of 29.8, extrusion speed of

3.93 mm/s and initial billet temperature 523 K (250 °C) were employed in these simulations. When the fraction factor values were 0 and 1, the temperature increments of extrudate were 124 K and 179 K (124 °C and 179 °C), respectively. The result was consistent with the above statement that the temperature increment during extrusion was partially attributed to the heat generation from severe friction between the billet and tooling.

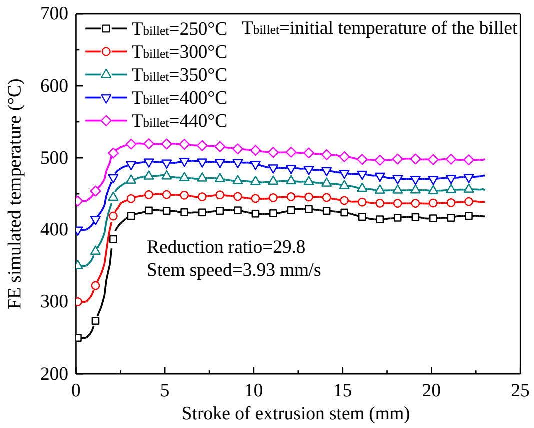

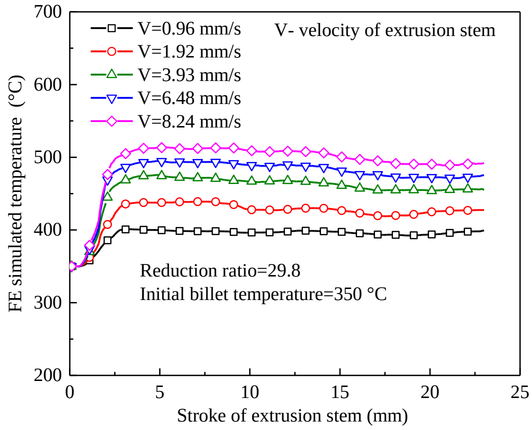

(a) (b)

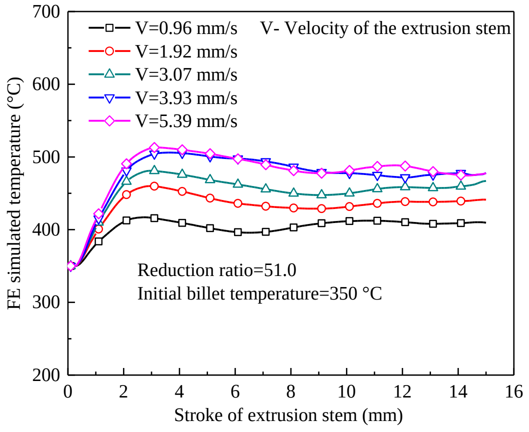

(c)

Fig. 6. FE simulated temperature evolutions at point P2 during extrusion: (a) at a reduction ratio of 29.8, stem speed of 3.93 mm/s and different initial billet temperatures, (b) at a reduction ratio of 29.8, initial billet temperature of 623 K (350 °C) and different stem speeds, and (c) at a reduction ratio of 51.0, initial billet temperature of 623 K (350 °C) and different stem speeds.

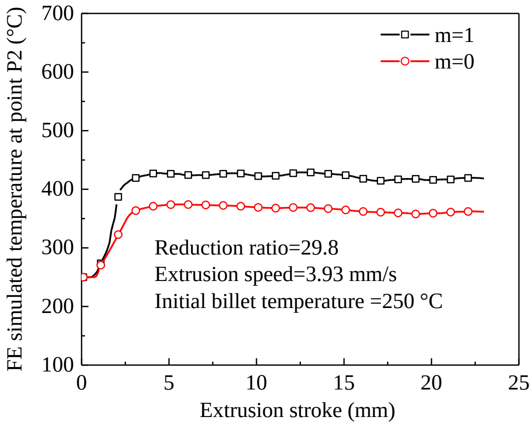

Fig. 7. Simulated temperatures at point P2 with friction factor values of 0 and 1.

When reduction ratio was 29.8 and stem speed 3.93 mm/s, the maximum extrudate temperatures reached 702, 723, 749 769 and 793 K (429, 450, 476, 496 and 520 °C) during extrusion at initial temperatures of 523, 573, 623, 673 and 713 K (250, 300, 350, 400 and 440 °C), respectively (Fig. 6a), meaning temperature increments of 179, 150, 126, 96 and 80 K (179, 150, 126, 96 and 80 °C), respectively. As the initial billet temperature increased, the temperature increment during extrusion decreased. This can be explained by the fact that the lower the initial billet temperature, the more heat generation from the higher flow stress of the magnesium alloy.

Fig. 6b shows the temperature evolutions at a reduction ratio of 29.8, initial billet temperature of 623 K (350 °C) and stem speeds of 0.96, 1.92, 3.93, 6.48 and 8.24 mm/s. The maximum temperature increments were 61, 89, 126, 145 and 154 K (61, 89, 126, 145 and 154 °C), respectively. With increasing extrusion speed, the maximum temperature of the extrudate grew. There are two factors that lead to the increases in extrudate temperature. On the one hand, the enhanced flow stress of the billet material at a higher extrusion speed leads to more heat generation than that at a lower extrusion speed. On the other hand, heat generation at a higher extrusion speed is less dissipated to the die.

When reduction ratio increased to 51.0 and the initial billet temperature remained unchanged (623 K, i.e., 350 °C), the maximum temperature increments were 67, 110, 131, 206 and 213 K (67, 110, 131, 206 and 213 °C), at stem speeds of 0.96, 1.92, 3.07, 3.93 and 5.39 mm/s, respectively (Fig. 6c). Comparison between the extrudate temperatures at these two reduction ratios (Fig. 6b and c) showed that a larger temperature increment appeared at a higher reduction ratio, but at the same initial billet temperature and extrusion speed. It can be explained by the fact that a higher strain rate at a larger reduction ratio contributes to the temperature increase of the extrudate.

3.2 Surface quality

The surface quality of an extruded magnesium alloy rod is negatively influenced by the defect of hot shortness. In general, the tendency for hot shortness to occur increases with increasing initial billet temperature, reduction ratio and extrusion speed. It is caused by an excessively high temperature due to heat generation inside the magnesium alloy undergoing large plastic deformation during extrusion. Figs. 8-10 show three groups of extruded magnesium alloy rods, which are arranged in a convenient way to demonstrate the influences of the initial billet temperature, extrusion speed and reduction ratio on the surface quality of the extruded rods.

Fig. 8 shows the magnesium alloy rods extruded at a reduction ratio of 29.8, stem speed of 3.93 mm/s and different initial billet temperatures. Defect-free surfaces of the extruded rods were obtained, when the initial billet temperatures were lower than 673 K (400 °C) (Fig. 8a-c). When the initial billet temperature increased to 673 K (400 °C), however, hot shortness occurred on the surface of the extruded rod (Fig. 8d). With a further increase in initial billet temperature to 713 K (440 °C), large and deep cracks on the surface of the extruded rod became visible to the naked eye (Fig. 8e). For the rods extruded under these conditions, FE simulation predicted the maximum extrudate temperatures T_e of 769 K and 793 K (496 °C and 520 °C). It could be inferred that the critical temperature for hot shortness to occur lay from 749 K to 769 K (476 °C to 496 °C). It was thus the initial billet temperature that influenced the surface quality of the extrudate [46, 47]. At the die bearing, tensile stresses due to severe friction exceeded the tensile strength of the material at the surface and consequently tearing occurred (Fig. 8d). If the heat generated from friction and hot deformation led to further temperature increases at the die bearing to the incipient melting point, localized melting took place, which would cause severe cracking on the surface (Fig. 8e).

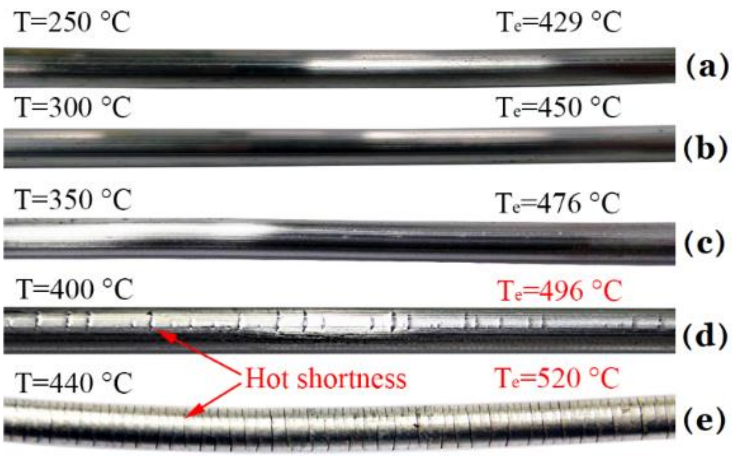

Fig. 8. Magnesium alloy rods extruded at a reduction ratio of 29.8, stem speed of 3.93 mm/s and different billet temperatures. T_e is the maximum extrudate temperature. (a) T=523 K (250 °C) and T_e=702 K (429 °C); (b) T=573 K (300 °C) and T_e=723 K (450 °C); (c) T=623 K (350 °C) and T_e=749 K (476 °C); (d) T=673 K (400 °C) and T_e=769 K (496 °C); (e) T=713 K (440 °C) and T_e=793 K (520 °C).

Extrusion speed is another factor influencing the surface quality of the extrudate, which embodies heat generation and dissipation during extrusion. It is obvious that heat generation increases with increasing extrusion speed, because a higher strain rate corresponds to more dynamic plastic deformation, and less heat is dissipated to the surrounding as a result of shortened process time, as shown in Fig. 6b. It is the raised extrudate temperature that limits the applicable extrusion speed. In the present research, at the same initial billet temperature of 623 K (350 °C) and reduction ratio of 29.8, the rods extruded at different stem speeds had different surface features (Fig. 9). When stem speeds were lower than 3.93 mm/s, the extruded magnesium alloy rods had smooth surface finish (Fig. 9a-c). When stem speed increased to 6.48 mm/s, however, minor cracks appeared on the surface of the extruded rod (Fig. 9d). Severe hot shortness occurred at the stem speed of 8.24 mm/s (Fig. 9e). FE simulations indicated the extrudate surface temperatures of 749, 768 and 787 K (476, 495 and 514 °C), at stem speeds of 3.93, 6.48 and 8.24 mm/s, respectively (Fig. 6b). In combination with the results shown earlier in Fig. 8d, the critical temperature for hot shortness to occur would be in the range of 749 K and 768 K (476 °C and 495 °C).

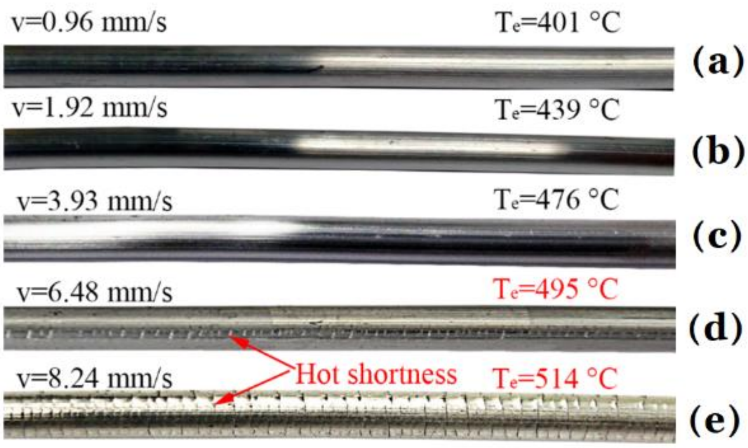

Fig. 9. Magnesium alloy rods extruded at a reduction ratio of 29.8, initial billet temperature of 623 K (350 °C) and different stem speeds. (a) v= 0.96 mm/s and T_e=674 K (401 °C); (b) v=1.92 mm/s

and T_e=712 K (439 °C); (c) v=3.93 mm/s and T_e=749 K (476 °C); (d) v=6.48 mm/s and T_e=768 K (495 °C); (e) v=8.24 mm/s and T_e=787 K (514 °C). T_e is the maximum extrudate temperature.

As mentioned earlier, heat generated from the plastic deformation of the billet material leads to the temperature rise of the extrudate. Reduction ratio is a process parameter that is directly related to the amount of plastic deformation. The extrusion experiments performed at a higher reduction ratio of 51.0 clearly depicted the effect of reduction ratio on extrudate surface quality (compare Fig. 10 and Fig. 9). When reduction ratio was 51.0, initial billet temperature 623 K (350 °C) and stem speed 3.93 mm/s, the maximum extrudate temperature reached 779 K (506 °C) and hot shortness occurred. At the lower reduction ratio of 29.8, however, the extrudate exhibited sound surface (Fig. 9c) and under this extrusion condition the maximum extrudate temperature was only 749 K (476 °C). It clearly indicated that the high reduction ratio increased the tendency of hot shortness. Fig. 10c shows the good surface of the extrudate at a stem speed of 3.07 mm/s and under this extrusion condition the extrudate temperature was 754 K (481 °C). By combining the results shown in Figs. 8, 9 and 10, one may infer the critical temperature for hot shortness to occur to be in the range of 754 K and 768 K (481 °C to 495 °C). The extrudate temperature of 754 K (481 °C) can be taken as a conservative critical temperature to avoid hot shortness.

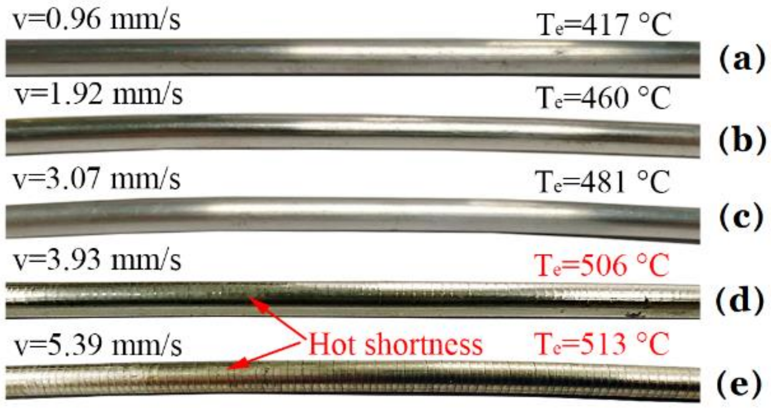

Fig. 10. Magnesium alloy rods extruded at a reduction ratio of 51.0, initial billet temperature of 623 K (350 °C) and different stem speeds. (a) v= 0.96 mm/s and T_e=987 K (417 °C); (b) v=1.92 mm/s and T_e=733 K (460 °C); (c) v=3.07 mm/s and T_e=754 K (481 °C); (d) v=3.93 mm/s and T_e=779 K (506 °C); (e) v=5.39 mm/s and T_e=786 K (513 °C). T_e is the maximum extrudate temperature.

3.3 Microstructures

Fig. 11 shows the microstructures of the as-cast and the as-solid-solution-treated Mg-Al-Zn-RE alloy. The as-cast alloy had a dendritic magnesium matrix and interdendritic second-phase particles (Fig. 11a). Morphology and composition analyses indicated the presence of four kinds of second-phase particles in the as-cast alloy, namely reticulate phase $Mg_{17}Al_{12}$, needle-like or lamellar phase $Al_{11}La_3$, and block-shaped phases Al_8Mn_5 and Al_2Gd (Figs. 11c, e-h and Table 4). $Mg_{17}Al_{12}$ and Al_8Mn_5 were the common intermetallic compounds in commercial Mg-Al-Zn alloys with a high Al content [48, 49]. $Al_{11}La_3$ and Al_2Gd were the compounds whose formation was due to the addition of rare earth elements of La and Ga [38, 50-51] to the Mg-Al-Zn base alloy. The volume fraction of second-phase particles in the SEM micrograph of the as-cast alloy was 7.3% (Fig. 11c). After the solid-solution treatment at 693 K (420 °C) for 24 h, the $Mg_{17}Al_{12}$ phase with a melting point of 701 K (437 °C) [40] disappeared due to its dissolution into the Mg matrix. The volume fraction of second-phase particles decreased significantly to 2.1% (Fig. 11d). During the heat treatment, the as-cast dendritic structure changed to an equiaxed grain structure; the mean grain size determined by using the linear intercept method [52] was 165 (±5) µm (Fig. 11b).

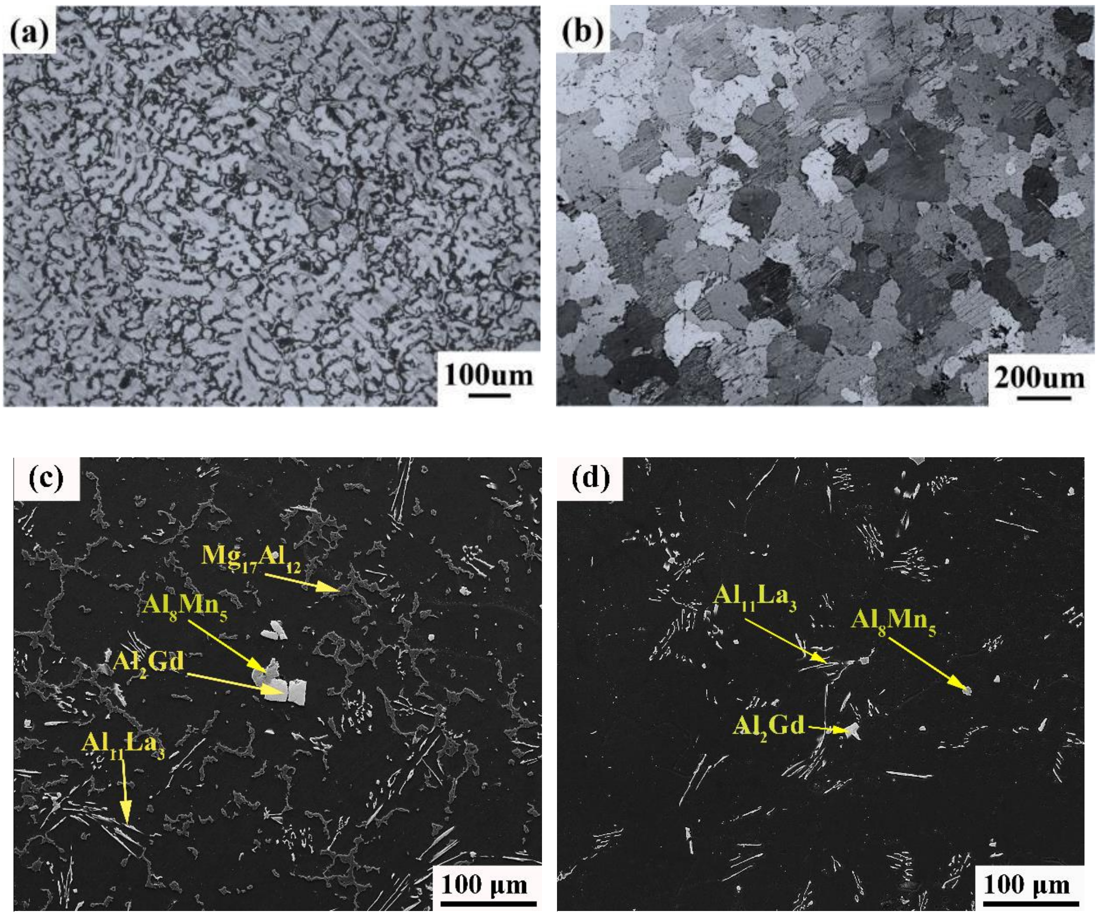

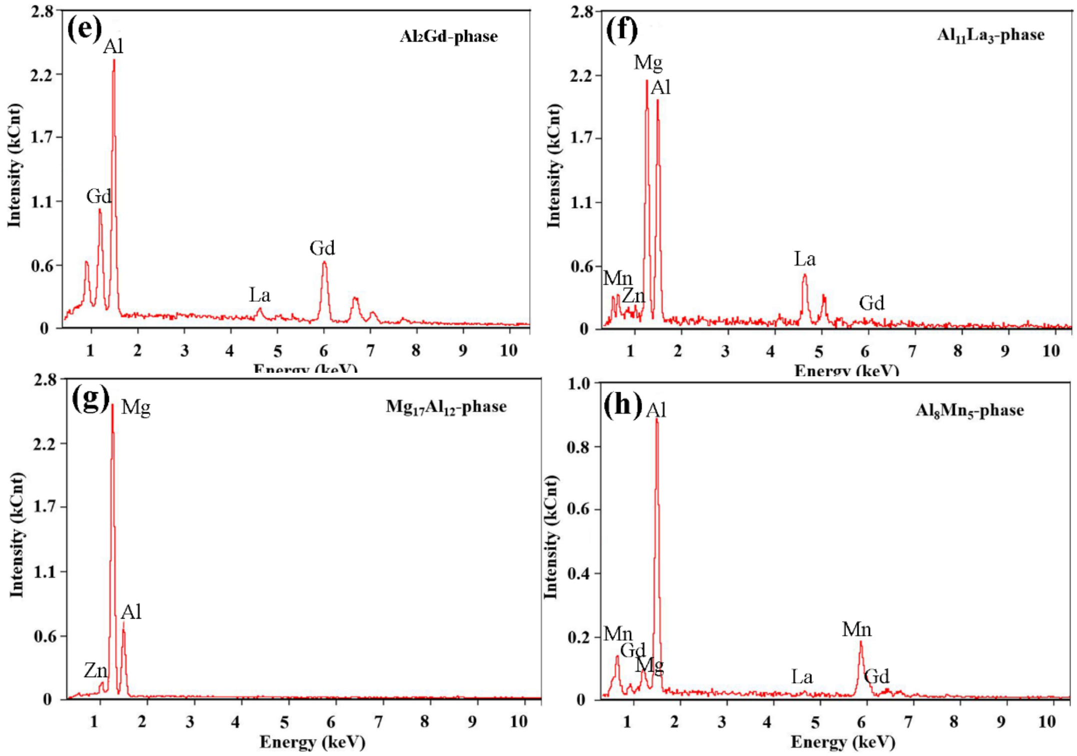

Fig. 11. Microstructures of the Mg-Al-Zn-RE alloy: (a) dendritic structure of the as-cast alloy; (b) equiaxed grain structure of the solid-solution-treated alloy; (c) SEM micrograph of the as-cast alloy; (d) SEM micrograph of the solid-solution treated alloy; (e-h) EDS element maps of Al_2Gd, $Al_{11}La_3$, $Mg_{17}Al_{12}$ and Al_8Mn_5 phases.

Table 4. EDS analysis of second-phase particles in the as-cast alloy.

Phases	Al_2Gd	$Al_{11}La_3$	$Mg_{17}Al_{12}$	Al_8Mn_5
Mg (at. %)		49.84	69.06	1.99
Al (at. %)	68.08	37.25	29.24	64.92
Zn (at. %)		0.78	1.70	
Mn (at. %)		0.41		25.70
La (at. %)	2.90	9.58		
Gd (at. %)	29.03	2.14		6.62

The optical microstructures of the magnesium alloy rods extruded at temperatures of 523-713 K (250-440 °C), a reduction ratio of 29.8 and stem speed of 3.93 mm/s are shown in Fig. 12. Apparently, dynamic recrystallization (DRX) occurred during extrusion under these conditions, and the mean grain sizes of the extruded magnesium alloy rods reduced significantly from the mean value of the as-solid-solution-treated alloy. The mean grain sizes of the rods extruded at 523, 573, 623, 673, 673 and 713 K (250, 300, 350, 400 and 440 °C) were 8.0 (±0.3), 8.5 (±0.5), 9.5 (±0.3), 10.9 (±0.3) and 12.4 (±0.4) μm, respectively, showing an increasing trend with rising initial billet temperature.

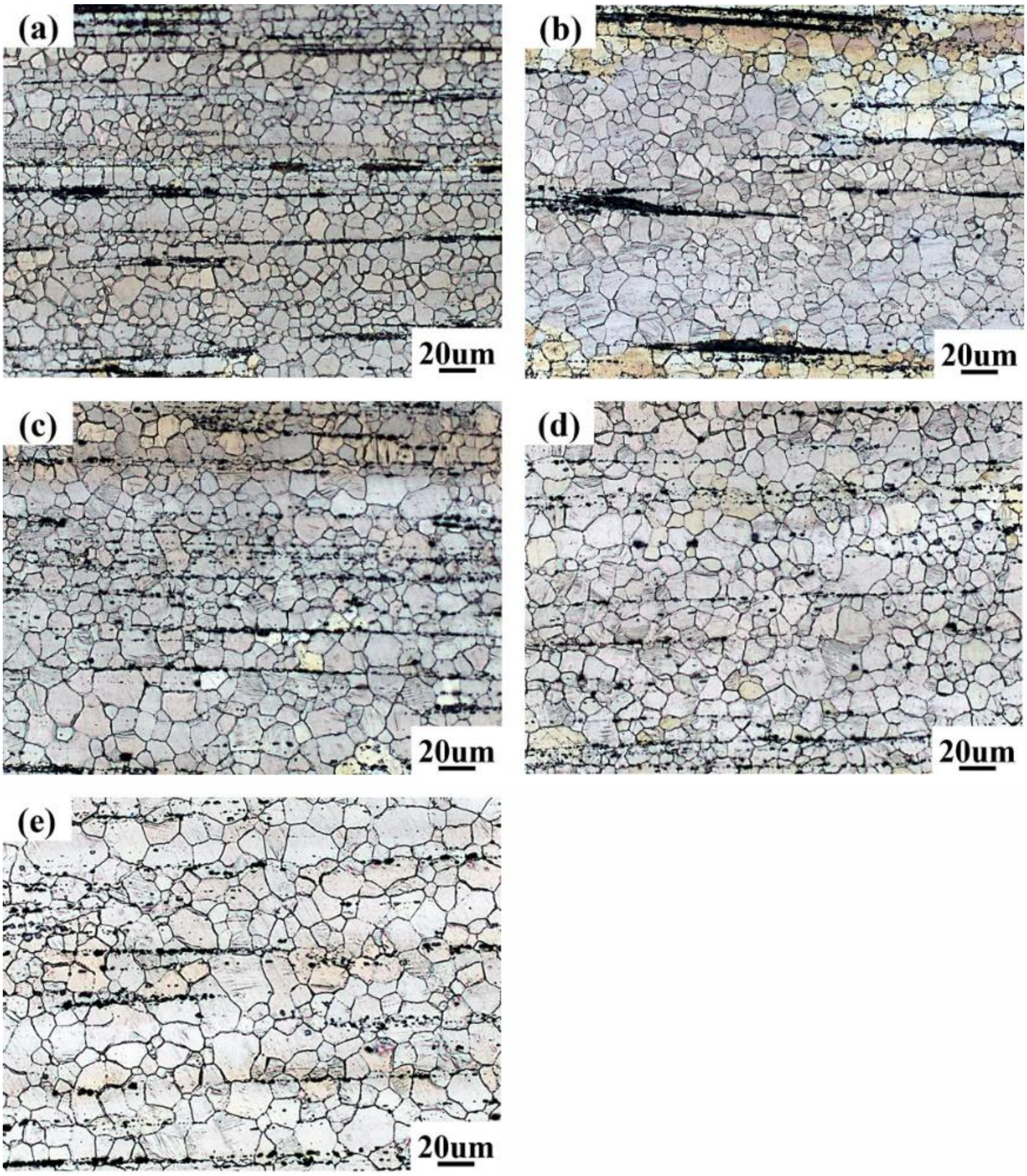

Fig. 12. Optical micrographs of the magnesium alloy rods extruded at a reduction ratio of 29.8, stem speed of 3.93 mm/s and initial billet temperatures of (a) 523, (b) 573, (c) 623, (d) 673 and (e) 713 K) [(a) 250, (b) 300, (c) 350, (d) 400 and (e) 440 °C].

The second phase $Mg_{17}Al_{12}$ reappeared due to dynamic precipitation from the supersaturated magnesium solid solution during extrusion and became distributed along the extrusion direction (Fig. 13). The needle-like or lamellar phase $Al_{11}La_3$ in the as-solid-solution-treated alloy was broken up and became block-shaped particles during extrusion. The sizes of second-phase particles increased, but their volume fraction decreased with increasing initial billet temperature. At the initial billet temperature of 523 K (250 °C), the maximum temperature of the extrudate reached 702 K (429 °C) and a lot of fine second-phase particles with sizes smaller than 1,000 nm were distributed on recrystallized grain boundaries (Figs.13a and c). The mean size of second-phase particles was 397 nm, and the volume fraction was 5.4%. At an increased initial billet temperature of 623 K (350 °C), the maximum temperature of the extrudate increased to 749 K (476 °C), the volume fraction of second-phase particles with sizes of 1,000 nm and larger increased and the mean size of second-phase particles increased to 492 nm. However, the overall volume fraction of second-phase particles decreased to 2.8% (Figs. 13b and d) as a result of higher solubility of the alloying elements in the magnesium matrix at a higher temperature. This phenomenon also was found in other magnesium alloys with high Al contents during extrusion [53, 54]. In addition to the dissolution of small particles, the alloying elements diffused and became accumulated at existing, larger particles, which resulted in particle growth.

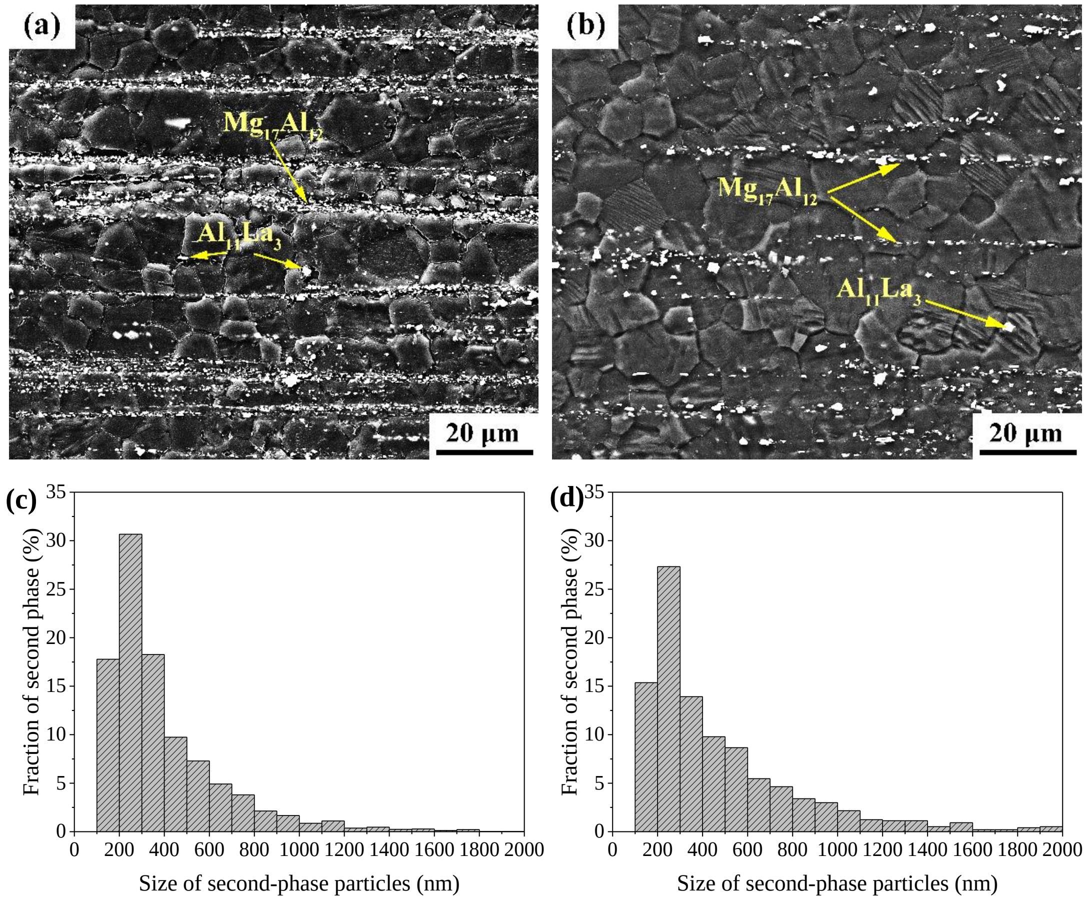

Fig. 13. SEM micrographs and distributions of the sizes of second-phases particles in the rods extruded at a reduction ratio of 29.8, stem speed of 3.93 mm/s and initial billet temperatures of (a) (c) 523 K (250 °C) and (b) (d) 623 K (350 °C).

Fig. 14 shows the optical micrographs of the magnesium alloy rods extruded at a billet temperature of 623 K (350 °C), reduction ratio of 29.8 and different stem speeds. With increases in stem speed from 0.96 to 1.92, 3.93, 6.48 and 8.24 mm/s, the mean grain sizes of the extruded magnesium rods rose marginally from 8.6 (±0.5) to 8.9 (±0.4), 9.5 (±0.3), 9.8 (±0.6) and 10.1 (0.5) μm, respectively. On the one hand, the extrudate temperature increased with increasing extrusion speed; the maximum extrudate temperature reached 674-787 K (401-514 °C) when stem speed increased from 0.96 to 8.24 mm/s (Fig. 6b). A high extrudate temperature would normally promote the growth of DRX grains. But on the other hand, the equivalent strain rate increased with increasing extrusion speed and a high strain rate would contribute to grain refinement during the hot deformation of magnesium alloys [55]. In addition, with increasing extrusion speed, the sizes and volume fraction of second-phase particles changed, which would affect grain sizes. Fig. 15 presents an SEM micrograph and a size distribution of second-phase particles in the magnesium alloy rod extruded at a reduction ratio of 29.8, initial billet temperature of 623 K (350 °C) and stem speed of 0.96 mm/s. The data could be compared with those obtained from the magnesium rod extruded at a higher stem speed of 3.93 mm/s, but at the same reduction ratio and initial billet temperature (Figs. 13b and d). With an increase in stem speed from 0.96 to 3.93 mm/s, the volume fraction of second-phase particles decreased from 3.6% to 2.8%, and the mean size decreased from 577 to 492 nm. The maximum extrudate temperature at stem speeds of 0.96 mm/s and 3.93 mm/s rose to 674 K to 745 K (401 °C and 472 °C), respectively. Clearly, it was the lower extrudate temperature at a lower extrusion speed that resulted in more and larger dynamically precipitated second-phase particles, as a result of longer time given for particle precipitation and growth. Comparison between Fig. 13d and Fig. 15b showed large volume fractions of second-phase particles smaller than 400 nm in the rods extruded at a higher extrusion speed, which would be highly effective to pin grain boundaries to retard grain growth.

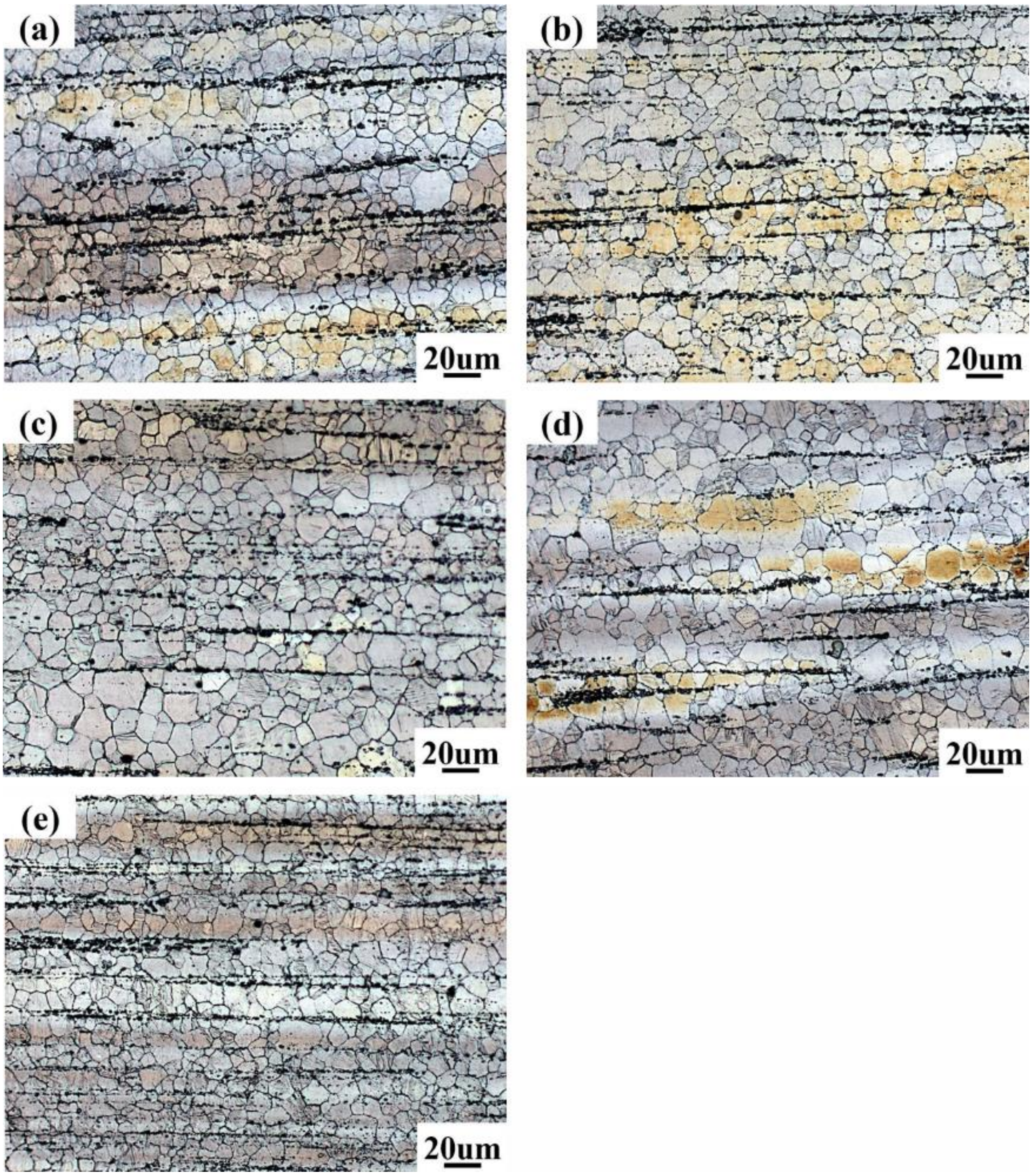

Fig. 14. Optical micrographs of the magnesium alloy rods extruded at a reduction ratio of 29.8, initial billet temperature of 623 K (350 °C) and stem speeds of (a) 0.96, (b) 1.92, (c) 3.93, (d) 6.48 and (e) 8.24 mm/s.

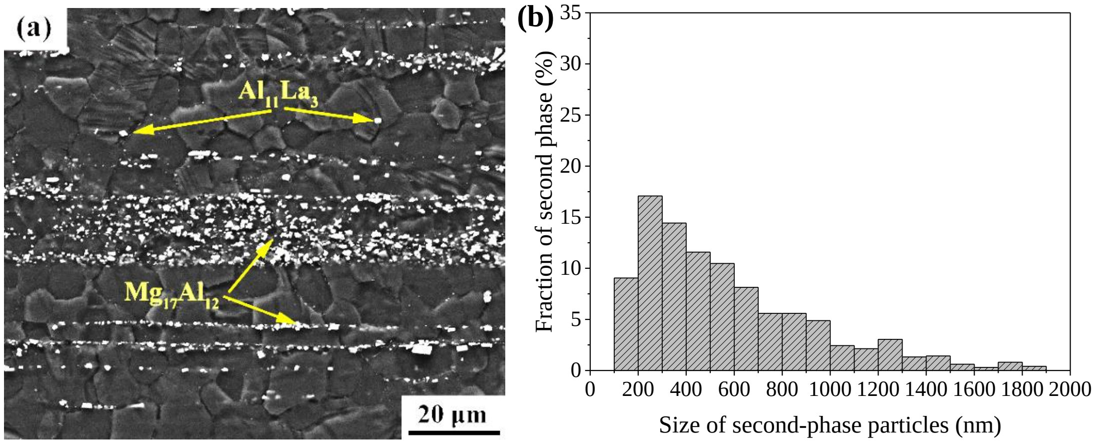

Fig. 15 SEM micrograph (a) and distribution of the size of second-phase particles (b) in the rods extruded at a reduction ratio of 29.8, stem speed of 0.96 mm/s and initial billet temperature of 623 K (350 °C).

The micrographs of the alloy extruded at the high reduction ratio of 51.0, presented in Fig. 16, were used to analyze the effect of reduction ratio on the microstructure of the extruded alloy. The initial billet temperature was 623 K (350 °C) and the stem speed was 0.96 mm/s. Comparison of the mean grain size obtained from Fig. 16a with that from Fig. 14a indicated a mild effect of reduction ratio from 29.8 to 51.0 on the mean grain size (from 8.6 to 9.4 µm). In addition, after extrusion at reduction ratios of 29.8 and 51.0, the volume fractions of second-phase particles were 3.6% and 2.9%, respectively, as a result of an increase in extrudate temperature.

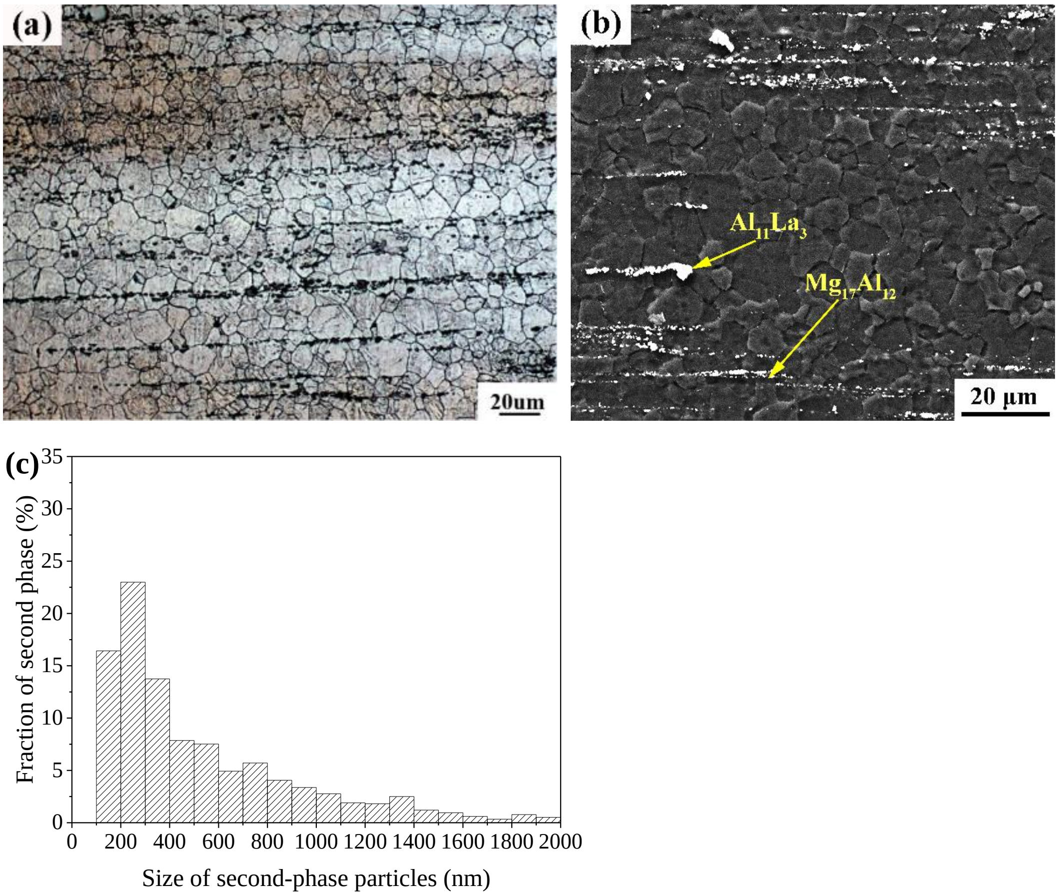

Fig. 16. Microstructures of the magnesium alloy rods extruded at an initial billet temperature of 623 K (350 °C), stem speed of 0.96 mm/s and reduction ratio of 51.0: (a) optical micrograph; (b) SEM micrograph; (c) distribution of the sizes of second-phase particles.

The size distributions and volume fractions of second-phase particles in Figs. 13, 15 and 16 were determined by using the software Image-Pro Plus on the basis of SEM micrographs at 2,000X magnification. With this method, nanoscale particles in the range of 1 and 100 nm were ignored, due to too low resolution. Fig. 17 presents a SEM micrograph at 20,000X magnification. The observed sample was extruded at an initial billet temperature of 623 K (250 °C), extrusion speed of 3.93 mm/s and a reduction ratio of 29.8. Nanoscale particles between 1 and 100 nm marked with arrows are clearly discernible. These tiny particles must have contributed to the improved strength of the extruded magnesium alloy as well, owing to precipitation strengthening.

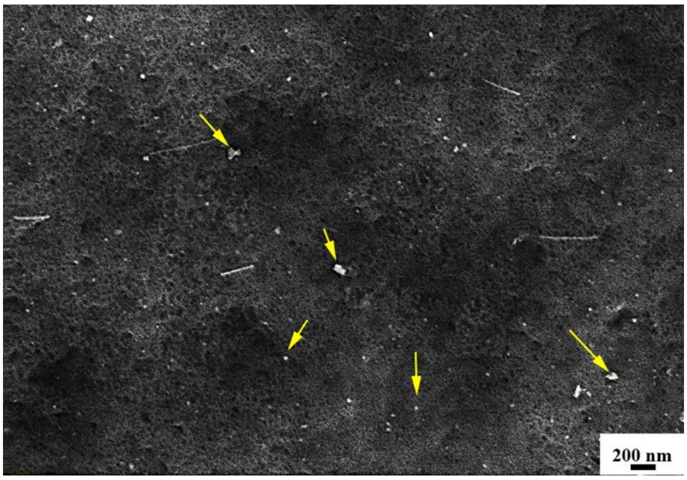

Fig. 17 SEM micrograph (20,000X) of the magnesium alloy rod extruded at an initial billet temperature of 523 K (250 °C), extrusion speed of 3.93 mm/s and a reduction ratio of 29.8.

In the present research, the mean grain sizes of the magnesium rods extruded under all the conditions ranged from 7 to 14 μm. The extrusion condition could influence the mean grain size of the magnesium alloy Mg-Al-Zn-RE to a certain extent, but the influence was quite moderate, in comparison with other magnesium alloys with low alloying contents. Zhang et al. [31], for example, reported that at a reduction ratio of 16 and extrusion speed of 4 mm/s, with an increase in billet temperature from 603 K to 673 K (330 °C to 400 °C), the mean grain size of the extruded Mg-1.0Zn-0.5Ca alloy increased from 2.5 μm to 25 μm. The main mechanism governing grain refinement during the hot deformation of a magnesium alloy is dynamic recrystallization (DRX), including the continuous DRX (CDRX) and discontinuous

DRX (DDRX) [55, 56]. DDRX, involving the nucleation and growth of new grains, was found to be the predominant mechanism in the magnesium alloy AZ31 [57]. Wang et al. [58] demonstrated that a larger value of the Zener-Hollomon parameter resulted in a higher ratio of nucleation rate to growth rate of new grains in the magnesium alloy ZM21, which was helpful for grain refinement. For these magnesium alloys with relatively low alloying contents, extrusion condition was found to influence the grain size of the extrudate strongly.

For the present magnesium alloy, abundant precipitates were present due to high contents of alloying elements added to magnesium. In addition to extrusion condition, precipitates would influence the DRX behavior of the alloy during extrusion. The precipitated $Mg_{17}Al_{12}$ phase and crushed $Al_{11}La_3$ phase would promote particle-stimulated nucleation (PSN) for DRX. These phases were mostly distributed on grain boundaries to exert the Smith-Zener pinning effect and restrict the growth of DRX grains [38]. Robson et al. [59] demonstrated that coarse, hard second-phase particles in Mg-Mn alloys, which promoted rapid sub-boundary migration during deformation, were necessary for the subsequent occurrence of PSN. Deng et al. [60] found that SiC particles of larger sizes (in the micrometer range) were more effective in promoting PSN of AZ91-SiC composites and refining grains than SiC particles of smaller sizes (in the sub-micrometer range). In the present investigation, second-phase particle sizes increased with increasing initial billet temperature and DRX via PSN would be more important. However, a higher temperature would weaken the nucleation via DDRX. The competition between these two effects made the mean grain size of the present alloy appear to be less sensitive to the initial billet temperature than that of the magnesium alloy Mg-1.0Zn-0.5Ca with low alloying contents [31].

As reported earlier, extrusion speed appeared to have a mild influence on the mean grain size of the present magnesium alloy. With increasing extrusion speed, the strain rate of the deforming billet and the extrudate temperature increased. A higher extrudate temperature would promote DRX grain growth, while a high strain rate would restrain DRX grain growth by increasing nucleation rates. As a net result, the direct influence of extrusion speed on the mean grain size became nearly invisible.

3.4 Mechanical properties

Fig. 18 shows the tensile stress-strain curves of the magnesium alloy rods extruded at different initial billet temperatures and extrusion speeds. Table 5 lists the tensile properties of the magnesium rods extruded at a reduction ratio of 29.8, together with mean grain sizes. After extrusion at initial billet temperatures of 523, 573, 623 and 673 K (250, 300, 350 and 400 °C) and a given stem speed of 3.93 mm/s, the extruded rods had ultimate tensile strengths (UTSs) of 397 ± 7, 387 ± 1, 384 ± 3 and 367 ± 7 MPa, 0.2% offset yield strengths (YSs) of 217 ± 3, 220 ± 5, 221 ± 1 and 221 ± 6 MPa, and elongation values of 20.8±1.3%, 18.2±0.4%, 15.8±0.4% and 13.6±0.4%, respectively. Clearly, both the UTS and the elongation decreased with rising initial billet temperature, which could be attributed to finer DRX grains at a lower initial billet temperature (Fig. 12 and Table 5). Precipitation strengthening, solid-solution strengthening, dislocation strengthening and subgrain strengthening might have contributed to the strength of the material extruded at a low temperature in addition to fine grain strengthening [38].

YS, UTS and elongation were only slightly improved by extrusion at a lower extrusion speed. At a given initial billet temperature of 623 K (350 °C), the material extruded at stem speeds of 0.96, 1.92 and 3.93 mm/s had the UTS values of 387±1, 386±4 and 384±3 MPa, the YS values of 226±4, 225±8 and 221±1 MPa, and elongation values of 17.0±1.4%, 16.6±0.5% and 15.8±0.4%, respectively (Table 5). The trends were consistent with the trend of the mean grain size varying with extrusion speed. It means that the scope to control the mean grain size and mechanical properties by varying extrusion speed appeared to be quite limited, which would give freedom to choosing extrusion speed for a higher production rate with only a little effect on the mechanical properties.

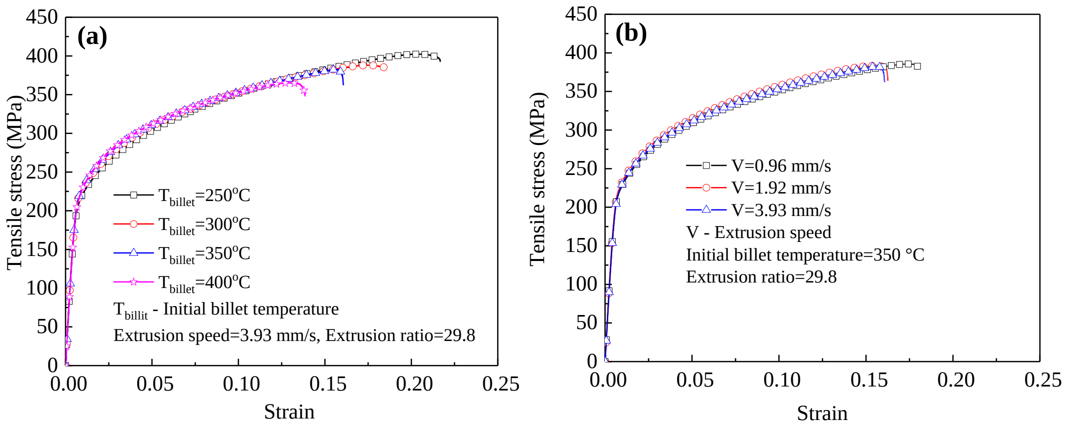

Fig. 18. Tensile stress-strain curves of the magnesium alloy rods extruded (a) at different billet temperatures and (b) at different extrusion speeds.

Table 5. Mechanical properties of the rods extruded at a reduction ratio of 29.8.

Stem speed (mm/s)	Billet temperature (°C)	UTS (MPa)	YS (MPa)	Elongation (%)	Mean grain size (μm)
3.93	250	397±7	217±3	20.8±1.3	8.0±0.3
	300	387±1	220±5	18.2±0.4	8.5±0.5
	350	384±3	221±1	15.8±0.4	9.5±0.3
	400	367±7	221±6	13.6±0.4	10.9±0.3
1.92	350	386±4	225±8	16.6±0.5	8.9±0.4
0.96	350	387±1	226±4	17.0±1.4	8.6±0.5

The ultimate tensile strengths (UTS), yield strengths (YSs) and mean grain sizes of selected Mg alloys are listed in Table 6 for comparison. It can be seen that the present alloy has a mean grain size similar to the mean grain sizes of the magnesium alloys AZ80 [34] and AZ80-1.52La-1.10Gd [61]. However, the present alloy has a higher UTS value than the other magnesium alloys of similar compositions. First of all, an optimized extrusion condition (reduction ratio: 29.8, initial billet temperature: 523 K

(250 °C) and ram speed: 3.93 mm/s) was employed to extrude the present alloy. Moreover, the addition of the rare earth elements raises the strengths of magnesium alloys. For example, Jiang et al. [50] found that over a Gd content range of 0.3% to 4%, the magnesium alloy AZ80 added with 0.9% Gd exhibited optimum mechanical properties. This was because coarse second phase particles were formed when excessive Gd was added to the magnesium alloy, thereby becoming detrimental to the mechanical properties. Over all, the magnesium alloy with high mechanical properties, both in UTS, YS and elongation, were obtained through adding rare earth elements to AZ80 and extrusion at the optimized condition.

Magnesium alloys with even finer grains and higher mechanical properties can be prepared through severe plastic deformation (SPD) [62, 63]. For example, Razavi et al. [63] demonstrated that via the multi-temperature (398 K to 473 K, i.e., 125 °C to 200 °C) equal-channel angular processing (ECAP) the magnesium alloy AZ31 exhibited extraordinarily high mechanical properties (YS =385 ± 6 MPa, UTS=455 ± 4 MPa, elongation=12.7%), owing to the ultra-fine grains (mean grain size=0.35 ± 0.10 um) formed during SPD. While the SPD process can significantly improve the mechanical properties of magnesium alloys, this process is only suitable for small-scale material preparation. With the industrial application taken into consideration, the commercial extrusion process may be more advantageous than the SPD process.

Table 6. Yield strengths, ultimate tensile strengths and mean grain sizes of selected Mg alloys for comparison.

Alloy (wt%)	UTS (MPa)	YS (MPa)	Mean grain size (um)	Extrusion condition		
				Reduction ratio	Initial billet temperature (°C)	Ram speed (mm/s)
AZ80 [34]	317-328	200-225	6-8	44	250-350	1
AZ80-1.52La-1.10Gd [61]	304-311	180-225	8.2-13.1	33.6	240-380	2
Mg-3Al-1Zn [63] *	455±4	385±6	0.35±0.10	-	-	-
AZ80-0.2Y-0.2Gd-0.1La [64]	306	264	12 ±2	10	380	-
AZ80-1.2Gd-0.8Nd [65]	325	262	-	10	-	-
AZ91-1Ca-0.5Si-0.1La-0.1Ce [66]	318	278	3	30	360	1.45
AZ91-0.3La [67]	330	180	-	17.4	350	1.7
Mg [68]	165	71	33	16.4	350	1.83
Mg-0.2Ce [68]	200-210	-	8	16.4	350	1.83
Mg-3Al [68]	226	105	23	16.4	350	1.83
AZ31 [69]	247	203	23	-	370	-
AM-EX1 [69]	259	184	7	-	370	-
Mg-(0.88-0.96) Mn-(0.32-2.11) Sr [70]	220-250	140-210	35-45	7	350	8
Present alloy (AZ80-1La-0.5Gd)	397±7	217±3	8.0±0.3	29.8	250	3.93

* The values were achieved through severe plastic deformation.

4. Conclusions

The extrudability and the effects of extrusion process parameters on the microstructure and mechanical properties of a new Mg-Al-Zn-RE alloy with large amounts of alloying elements were investigated by means of extrusion experiments and FE simulations. The following conclusions could be drawn.

(1) Hot shortness was the main defect negatively affecting the surface quality of the extruded magnesium alloy. The tendency for hot shortness to occur increased with increasing initial billet temperature, extrusion speed and reduction ratio. The critical temperature for hot shortness to occur was found to be between 754 K and 768 K (481 °C and 495 °C).

(2) DRX occurred during hot extrusion and grains were significantly refined. The mean grain size of the extruded alloy decreased with decreasing initial billet temperature. An increase in extrusion speed and reduction ratio only slightly promoted DRX grain growth. Fine grains with a mean size of 8.0 (±0.3) μm were present in the alloy extruded at an initial billet temperature of 523 K (250 °C), stem speed of 3.93 mm/s and reduction ratio of 29.8.

(3) The $Mg_{17}Al_{12}$ phase dynamically precipitated during extrusion from the supersaturated magnesium matrix after the solid solution treatment. The $Al_{11}La_3$ phase was crushed during extrusion. A large number of second-phase particles with sizes smaller than 1.0 μm were distributed on grain boundaries. The volume fraction of second-phase particles decreased with rising extrudate temperature. These particles aided in DRX grain refinement through particle-stimulated nucleation and grain boundary pinning.

(4) The UTS and elongation of the extruded rod increased with decreasing initial billet temperature and extrusion speed. The extruded rod with an optimum combination of mechanical properties (YS=217±3 MPa, UTS=397±7 MPa and

elongation=20.8% (±1.3%)) was obtained at an initial billet temperature of 523 K (250 °C), stem speed of 3.93 mm/s and reduction ratio of 29.8 mainly as a result of a refined grain structure.

Acknowledgements

The authors (Gang Fang and Sheng-Wen Bai) greatly appreciate the financial support of the National Natural Science Foundation of China (Project No.51675300).

References

[1] M.K. Kulekci, Int. J. Adv. Manuf. Tech., 2008, vol. 39, pp. 851-865.

[2] A.A. Luo, Int. Mater. Rev., 2004, vol. 49, pp. 13-30.

[3] E.F. Volkova, Met. Sci. Heat Treat., 2006, vol. 48, pp. 473-478

[4] S. Yao, Y.F. Li, Sci. Total Environ., 2015, vol. 44, pp. 89-96.

[5] H. Pan, Y. Ren, H. Fu, H. Zhao, L. Wang, X. Meng, G. Qin, J. Alloy. Compd., 2016, vol. 663, pp. 321-331.

[6] D. Letzig, J. Swiostek, J. Bohlen, P. A. Beaven, K.U. Kainer, Metal Science J., 2013, vol. 24, pp. 991-996.

[7] A.A. Luo, J. Magn. Alloy., 2013, vol. 1, pp. 2-22.

[8] W. A. Monteiro, S. J. Buso, L. V. da Silva, Application of magnesium alloys in transport, in: W.A. Monteiro (Ed.), New Features on Magnesium Alloys, InTech, Rijeka, 2012, pp. 1-14.

[9] S. You, Y. Huang, K.U. Kainer, N. Hort, J. Magn. Alloys, 2017, vol. 5, pp. 239-253.

[10] Z. Zeng, N. Stanford, C.H.J. Davies, J.F. Nie, N. Birbilis, Int. Mater. Rev., 2018, vol. 2, pp. 1-36.

[11] C. Bettles, M. Barnett, Advances in Wrought Magnesium Alloys: Fundamentals of Processing, Properties and Applications, Woodhead Publishing, Philadelphia, PA, USA, 2012, pp. 304-322.

[12] D.S. Yin, E.L. Zhang, S.Y. Zeng, Trans. Nonferr Metal. Soc., 2008, vol. 18, pp. 763-768.

[13] W.N. Tang, S.S. Park, B.S. You, Mater. Des., 2011, vol. 32, pp. 3537-3543.

[14] S. M. Masoudpanah, R. Mahmudi, Mater. Sci. Eng., 2009, vol. A526, pp. 22-30.

[15] B. Zhang, Y. Wang, L. Geng, C. Lu, Mater. Sci. Eng. A, 2012, vol. 539, pp. 56-60.

[16] J. Bohlen, S. Yi, D. Letzig, K.U. Kainer, Mater. Sci. Eng. A, 2010, vol. 527, pp. 7092-7098.

[17] D.K. Xu, W.N. Tang, L. Liu, Y.B. Xu, E.H. Han, J. Alloy. Compd., 2007, vol. 432, pp. 129-134.

[18] D.K. Xu, L. Liu, Y.B. Xu, E.H. Han, J. Alloy. Compd., 2006, vol. 426, pp. 155-161.

[19] N. Stanford, M. R. Barnett, Mater. Sci. Eng. A, 2008, vol. 496, pp. 399-408.

[20] M. Yamasaki, K. Hashimoto, K. Hagihara, Y. Kawamura, Acta Mater., 2011, vol. 59, pp. 3646-3658.

[21] X. Li, W. Qi, K. Zheng, N. Zhou, J. Magn. Alloys, 2013, vol. 1, pp. 54-63.

[22] X. Zeng, Y. Zhang, C. Lu, W. Ding, Y. Wang, Y. Zhu, J. Alloy. Compd., 2005, vol. 395, pp. 213-219.

[23] N. Stanford, D. Atwell, M. R. Barnett, Acta Mater., 2010, vol. 58, pp. 6773-6783.

[24] J.B. Zhang, L.B. Tong, C. Xu, Z.H. Jiang, L.R. Cheng, S. Kamado, H.J. Zhang, Mater. Sci. Eng. A, 2017, vol. 708, pp. 11-20.

[25] T. Homma, N. Kunito, S. Kamado, Scripta Mater., 2009, vol. 61, pp. 644-647.

[26] M. Yamasaki, T. Anan, S. Yoshimoto, Y. Kawamura, Scripta Mater., 2005, vol. 53, pp. 799-803.

[27] Y. Chen, L. Hao, Y. Ruiyu, G. Liu, T. Xia, Mater. Sci. Technol., 2014, vol. 30, pp. 495-500.

[28] A. A. Luo, C. Zhang, A. K. Sachdev, Scripta Mater., 2012, vol. 66, pp. 491-494.

[29] T. Murai, S.I. Matsuoka, S. Miyamoto, Y. Oki, J. Mater. Process. Technol., 2001, vol. 141, pp. 207-212.

[30] S. Ishihara, H. Shibata, K. Komano, T. Goshima, Z.Y. Nan, Key Eng. Mater., 2007, vol. 353, pp. 291-294.

[31] B.P. Zhang, L. Geng, L.J. Huang, X.X Zhang, C.C. Dong, Scripta Mater., 2010, vol. 63, pp. 1024-1027.

[32] L.B. Tong, M.Y. Zheng, L.R. Cheng, D.P. Zhang, S. Kamado, J. Meng, H.J. Zhang, Mater. Charact., 2015, vol. 104, pp. 66-72.

[33] S.H. Park, J.G. Jung, Y.M. Kim, B.S. You, Mater. Lett., 2015, vol. 139, pp. 35-38.

[34] M. Shahzad, L. Wagner, Mater. Sci. Eng. A, 2009, vol. 506, pp. 141-147.

[35] Q. Chen, D. Shu, Z. Zhao, Z. Zhao, Y. Wang, B. Yuan, Mater. Des., 2012, vol. 40, pp. 488-496.

[36] A. Singh, Y. Osawa, H. Somekawa, H. Somekawa, T. Mukai, C.J. Parrish, D.S. Shih, Metall. Mater. Trans. A, 2014, vol. 45, pp. 3232-3240.

[37] S.H. Park, J.H. Bae, S.H. Kim, J. Yoon, B.S. You, Metall. Mater. Trans. A, 2015, vol. 46, pp. 5482-5488.

[38] F. Bu, Q. Yang, K. Guan, X. Qiu, D. Zhang, W. Sun, J. Alloy. Compd., 2016, vol. 688, pp. 1241-1250.

[39] X. Luo, S. Dang, L. Kang, Adv. Mater. Sci. Eng., 2014, vol. 2014, pp. 1-7.

[40] J. Mohammadi, M. Ghoreishi, Y. Behnamian, Mater. Res., 2014, vol. 17, pp. 994-1002.

[41] C.M. Sellars, W.J. McTegart, Acta Metall., 1966, vol. 14, pp. 1136–38

[42] L. Li, H. Zhang, J. Zhou, J. Duszczyk, G. Li, Z.H. Zhong, Mater. Des., 2008, vol. 29, pp. 1190-1198.

[43] G. Liu, J. Zhou, J. Duszczyk, J. Mater. Process. Technol., 2008, vol. 200, pp. 185-198.

[44] L. Li, J. Zhou, and J. Duszczyk, J. Mater. Process. Technol., 2006, vol. 172, pp. 372–80.

[45] J. Zhou, L. Li, J. Duszczyk, J. Mater. Process. Technol., 2003, vol. 134, pp. 383-397.

[46] T. Sheppard, Extrusion of Aluminum Alloys, Kluwer Academic Publishers, Dordrecht, The Netherlands, 1999, pp. 227–52.

[47] M.P. Clade, T. Sheppard, Mater. Sci. Technol., 1993, vol. 9, pp. 313-318.

[48] W. Wei, C. Xu, J. Zhang, X. Niu, China Foundry, 2014, vol. 11, pp. 157-162.

[49] Y.S. Yang, J.C. Wang, T. Wang, C.M. Liu, Z.M. Zhang, Trans. Nonferr Metal. Soc., 2014, vol. 24, pp. 76-81.

[50] N. Jiang, L.G. Meng, X.G. Zhang X G, L. Chen, C.F. Fang, H. Hao, Rare Met., 2017, pp. 1-7.

[51] X.D. Wang, W.B. Du, K. Liu, Z.H. Wang, S.B. Li, J. Alloys Comp., 2012, vol. 522, pp. 78– 84.

[52] J.C. Wurst, J.A. Nelson, J. Am. Ceram. Soc., 1972, vol. 55, pp. 109-109.

[53] H. Ding, L. Liu, S. Kamado, D. Wang, Y. Kojima, J. Alloy. Compd., 2008, vol. 456, pp. 400-406.

[54] S.W Xu, N. Matsumoto, S. Kamado, T. Honma, Y. Kojima, Scripta Mater., 2009, vol. 61, pp. 249-252.

[55] S.M. Fatemi-Varzaneh, A. Zarei-Hanzaki, H. Beladi, Mater. Sci. Eng. A, 2007, vol. 456, pp. 52-57.

[56] O. Sitdikov, R. Kaibyshev, Mater. Trans., 2001, vol. 42, pp. 1928-1937.

[57] A.G. Beer, M.R. Barnett, Metall. Mater. Trans. A, 2007, vol. 38, pp. 1856-1867.

[58] L. Wang, G. Fang, L. Qian, Mater. Sci. Eng. A, 2018, vol. 711, pp. 268-283.

[59] J.D. Robson, D.T. Henry, B. Davis, Acta Mater., 2009, vol. 57, pp. 2739-2747.

[60] K.K. Deng, X.J. Wang, Y.W. Wu, X.S. Hu, K. Wu, W.M. Gan, Mater. Sci. Eng. A, 2012, vol. 543, pp. 158-163.

[61] Q. Liao, X. Chen, Q. Lan, F. Ning, Q. Le, Mater. Res. Express, 2018, vol. 5, pp. 1-10.

[62] D.C. Foley, M. Al-Maharbi, K.T. Hartwig, I. Karaman, L.J. Kecskes, S.N. Mathaudhu, Scripta Mater., 2011, vol. 64, pp. 193-196.

[63] S.M. Razavi, D.C. Foley, I. Karaman, K.T. Hartwig, O. Duygulu, L.J. Kecskes, S.N. Mathaudhu, V.H. Hammond, Scripta Mater., 2012, vol. 67, pp. 439-442.

[64] K. Cai, Z. Gao, Q. Zhu, Y. Jin, Y. Chai, D. Fang, Rare Metal Mater. Eng., 2015, vol. 44, pp. 1489-1493.

[65] Q. Zhu, C. Fang, N. Li, L. Meng, Y. Wang, Y. Wu, X. Zhang, Rare Metal Mater. Eng., 2013, vol. 42, pp. 771-775.

[66] C. Che, Z. Cai, X. Yang, L. Cheng, Y. Du, Mater. Sci. Eng. A, 2017, vol. 705, pp. 282-290.

[67] L. Fu, X.B. Wang, P.L. Gou, Q.C. Le, W. T. Jia, Y. Tang, Adv. Eng. Mater., 2017, vol. 19, pp. 1700230.

[68] A.A. Luo, W. Wu, R.K. Mishra, L. Jin, A.K. Sachdev, W. Ding, Metall. Mater. Trans. A, 2010, vol. 41, pp. 2662-2674.

[69] M. Easton, A. Beer, M. Barnett, C. Davies, G. Dunlop, Y. Durandet, S. Blacket, T. Hilditch, P. Beggs, JOM, 2008, vol. 60, pp. 57-62.

[70] H. Borkar, M. Hoseini, M. Pekguleryuz, Mater. Sci. Eng. A, 2012, vol. 549, pp. 168-175.

Table and figure captions

Table 1. Nominal chemical composition (wt.%) of the Mg-Al-Zn-RE alloy.

Table 2. Constitutive constants of the magnesium alloy (Mg-Al-Zn-RE).

Table 3. Physical properties of the billet and extrusion tooling.

Table 4. EDS analysis of second-phase particles in the as-cast alloy.

Table 5. Mechanical properties of the rods extruded at a reduction ratio of 29.8.

Table 6. Yield strengths, ultimate tensile strengths and mean grain sizes of selected Mg alloys for comparison.

Fig. 1. Flow stress curves of the magnesium alloy at temperatures from 773 K to 693 K (300 °C to 420 °C) and strain rates (a) 0.001 s^{-1}, (b) 0.01 s^{-1}, (c) 0.1 s^{-1}, (d) 1 s^{-1} and (e) 10 s^{-1}.

Fig. 2. Tooling set-up to extrude rods: (a) schematic and (b) dimensions of one of the extrusion dies.

Fig. 3. Schematic of the longitudinal section of an extruded rod for microstructure observation.

Fig. 4. Axisymmetric FE model to simulate the extrusion process to produce rods.

Fig. 5. Predicted temperature distribution inside the billet, extrudate and extrusion tooling (a) and comparison between the measured and predicted temperatures at P1 along with stem displacement (b).

Fig. 6. FE simulated temperature evolutions at point P2 during extrusion: (a) at a reduction ratio of 29.8, stem speed of 3.93 mm/s and different initial billet temperatures, (b) at a reduction ratio of 29.8, initial billet temperature of 623 K (350 °C) and different stem speeds, and (c) at a reduction ratio of 51.0, initial billet temperature of 623 K (350 °C) and different stem speeds.

Fig. 7. Simulated temperatures at point P2 with friction factor values of 0 and 1.

Fig. 8. Magnesium alloy rods extruded at a reduction ratio of 29.8, stem speed of 3.93 mm/s and different billet temperatures. (a) T=523 K (250 °C) and T_e=702 K (429 °C); (b) T=573 K (300 °C) and T_e=723 K (450 °C); (c) T=623 K (350 °C) and T_e=749 K (476 °C); (d) T=673 K (400 °C) and T_e=769 K (496 °C); (e) T=713 K (440 °C) and T_e=793 K (520 °C). T_e is the maximum extrudate temperature.

Fig. 9. Magnesium alloy rods extruded at a reduction ratio of 29.8, initial billet temperature of 623 K (350 °C) and different stem speeds. (a) v= 0.96 mm/s and T_e=674 K (401°C); (b) v=1.92 mm/s and T_e=712 K (439 °C); (c) v=3.93 mm/s and T_e=749 K (476 °C); (d) v=6.48 mm/s and T_e=768 K (495 °C); (e) v=8.24 mm/s and T_e=787 K (514°C). T_e is the maximum extrudate temperature.

Fig. 10. Magnesium alloy rods extruded at a reduction ratio of 51.0, initial billet temperature of 623 K (350 °C) and different stem speeds. (a) v= 0.96 mm/s and T_e=690 K (417 °C); (b) v=1.92 mm/s and T_e=733 K (460 °C); (c) v=3.07 mm/s and T_e=754 K (481°C); (d) v=3.93 mm/s and T_e=779 K (506 °C); (e) v=5.39 mm/s and Te=786 K (513 °C). T_e is the maximum extrudate temperature.

Fig. 11. Microstructures of the Mg-Al-Zn-RE alloy: (a) dendritic structure of the as-cast alloy; (b) equiaxed grain structure of the solid-solution-treated alloy; (c) SEM micrograph of the as-cast alloy; (d) SEM micrograph of the solid-solution treated alloy; (e-h) EDS element maps of Al_2Gd, $Al_{11}La_3$, $Mg_{17}Al_{12}$ and Al_8Mn_5 phases.

Fig. 12. Optical micrographs of the magnesium alloy rods extruded at a reduction ratio of 29.8, stem speed of 3.93 mm/s and initial billet temperatures of (a) 523, (b) 573, (c) 623, (d) 673 and (e) 713 K [(a) 250, (b) 300, (c) 350, (d) 400 and (e) 440 °C].

Fig. 13. SEM micrographs and distributions of the sizes of second-phases particles in the rods extruded at a reduction ratio of 29.8, stem speed of 3.93 mm/s and initial billet temperatures of (a) (c) 523 K (250 °C) and (b) (d) 623 K (350 °C).

Fig. 14. Optical micrographs of the magnesium alloy rods extruded at a reduction ratio of 29.8, initial billet temperature of 623 K (350 °C) and stem speeds of (a) 0.96, (b) 1.92, (c) 3.93, (d) 6.48 and (e) 8.24 mm/s.

Fig. 15. SEM micrograph (a) and distribution of the size of second-phase particles (b) in the rods extruded at a reduction ratio of 29.8, stem speed of 0.96 mm/s and initial billet temperature of 623 K (350 °C).

Fig. 16. Microstructures of the magnesium alloy rods extruded at an initial billet temperature of 623 K (350 °C), stem speed of 0.96 mm/s and reduction ratio of 51.0: (a) optical micrograph; (b) SEM micrograph; (c) distribution of the sizes of second-phase particles.

Fig. 17. SEM micrograph (20,000X) of the magnesium alloy rod extruded at an initial billet temperature of 523 K (250 °C), extrusion speed of 3.93 mm/s and a reduction ratio of 29.8.

Fig. 18. Tensile stress-strain curves of the magnesium alloy rods extruded (a) at different billet temperatures and (b) at different extrusion speeds.